

Dynamics of triple black hole systems in hierarchically merging massive galaxies

Loren Hoffman¹* and Abraham Loeb²†

¹Physics Department, Harvard University, 17 Oxford St., Cambridge, MA 02138, USA

²Astronomy Department, Harvard University, 60 Garden Street, Cambridge, MA 02138, USA

24 December 2018

ABSTRACT

Galaxies with stellar bulges are generically observed to host supermassive black holes (SMBHs). The hierarchical merging of galaxies should therefore lead to the formation of SMBH binaries. Merging of old massive galaxies with little gas promotes the formation of low-density nuclei where SMBH binaries are expected to survive over long times. If the binary lifetime exceeds the typical time between mergers, then triple-black-hole systems may form. Such systems can lead to the ejection of one of the black holes (BHs) at a speed exceeding 10^3 km s $^{-1}$, far greater than attainable through gravitational radiation recoil. We study the statistics of close triple-SMBH encounters in galactic nuclei by computing a series of three-body orbits with physically-motivated initial conditions appropriate for giant elliptical galaxies. Our simulations include a smooth background potential consisting of a stellar bulge plus a dark matter halo, drag forces due to gravitational radiation and dynamical friction on the stars and dark matter, and a simple model of the time evolution of the inner density profile under heating and mass ejection by the SMBHs. We find that the binary pair coalesces as a result of repeated close encounters in $\sim 85\%$ of our runs, and in $\sim 15\%$ of cases a new eccentric binary forms from the third SMBH and binary remnant and coalesces during the run time. In about 40% of the runs the lightest BH is left wandering through the galactic halo or escapes the galaxy altogether, but escape of all three SMBHs is exceedingly rare. The triple systems typically scour out cores with mass deficits $\sim 1\text{--}2 \times$ their total mass, which can help to account for the large cores observed in some massive elliptical galaxies, such as M87. The high coalescence rate, prevalence of very high-eccentricity orbits, and gravitational radiation “spikes” during close encounters in our runs, may provide interesting signals for the future Laser Interferometer Space Antenna (LISA).

Key words: black hole physics—cosmology: theory—galaxies: elliptical and lenticular, cD—galaxies: evolution—galaxies: interactions—galaxies: nuclei

1 INTRODUCTION

In the favored cold dark matter cosmology, present-day galaxies were assembled hierarchically from smaller building blocks at earlier cosmic times. Since all nearby galaxies with stellar spheroids are observed to host nuclear SMBHs (Kormendy & Gebhardt 2001), hierarchical merging leads inevitably to the formation of SMBH binaries (Begelman et al. 1980). If the binary lifetime exceeds the typical time between mergers, then some galactic nuclei should contain systems of three or more SMBHs. In this paper we simulate the dynamics of triple SMBH systems. These systems are particularly interesting as they can lead

to the ejection of one of the BHs at a speed comparable to the galactic escape velocity (Hoffman & Loeb 2006). In massive elliptical galaxies the typical speeds are $\sim 10^3$ km s $^{-1}$, far greater than attainable through gravitational radiation recoil (Centrella 2006; Favata et al. 2004; Blanchet et al. 2005).

While the characteristic mass of cold dark matter halos tends to increase with cosmic time, that of *actively star forming* galaxies is actually observed to *decrease* with time (Cowie et al. 1996). This “downsizing” trend leads to passive evolution of large galaxies at late times – essentially collisionless merging in which the gravitational signature imprinted on the stellar distribution persists indefinitely. While this makes such luminous signatures of major mergers as starbursts and bright quasars less prevalent, it permits the formation of low-density nuclei with longer relaxation times

* E-mail:lhoffman@cfa.harvard.edu

† E-mail:aloeb@cfa.harvard.edu

in which SMBH binaries may have lifetimes exceeding the age of the universe.

Spatially resolved pairs of nuclei have been observed in a few active galaxies. The most famous example is NGC 6240, an Ultraluminous Infrared Galaxy (ULIRG) in which two distinct active galactic nuclei (AGN) are clearly seen in hard X-rays at a projected separation of ~ 1 kpc (Komossa et al. 2003). Maoz et al. (1995, 2005) observed a variable UV source, possibly a second active nucleus, at a projected separation of ~ 60 pc from the primary nucleus in the spiral galaxy NGC 4736, which shows signs of a recent merger. Rodriguez et al. (2006) have detected what is thought to be an SMBH binary at a projected separation of 7.3 pc in the radio galaxy 0402+379 through multi-frequency radio observations using the Very Long Baseline Array (VLBA). We begin by discussing the theory of how such systems evolve, and the conditions under which they might acquire a third BH, leading to the motivation for this paper and its outline.

1.1 Black hole binaries

When two galaxies merge, their dense nuclei sink to the center of the merger product by dynamical friction. As the nuclei spiral in, tidal forces gradually strip the two SMBHs of their surrounding stars and dark matter. In mergers between galaxies of comparable mass, the BHs are able to come together and form a bound SMBH binary on a timescale of order 10^9 yrs. The binary continues to harden by dynamical friction until it reaches a separation of order

$$a_{\text{hard}} \equiv \frac{G\mu}{4\sigma^2} \approx 1.6 \frac{2q}{(1+q)^2} \left(\frac{m_{\text{bin}}}{10^8 M_{\odot}} \right)^{1/2} \text{ pc}, \quad (1)$$

known as the “hardening radius” (e.g. Quinlan 1996). Here $\mu = m_1 m_2 / (m_1 + m_2)$ is the reduced mass of the two BHs with masses m_1 and m_2 , σ is the velocity dispersion of the stars beyond the binary’s sphere of gravitational influence, q is the binary mass ratio $m_2/m_1 \leq 1$, and $m_{\text{bin}} = m_1 + m_2$ is the total mass of the binary. For smaller separations the binary looks like a point mass to the distant stars contributing to dynamical friction, but close stellar encounters preferentially harden the binary and so dominate further energy loss. Only stars on nearly radial orbits, with pericenter distances of order the binary separation, can extract energy from (“harden”) the binary in this stage. These stars undergo strong three-body interactions with the binary and escape its vicinity with speeds comparable to the black holes’ orbital speed. In the low-density nuclei of large elliptical galaxies, the total mass in stars on such “loss cone” orbits is small compared to the mass of the binary. Furthermore the two-body stellar relaxation time is long compared to a Hubble time, so once the stars initially on loss cone orbits are cleared out, the loss cone remains empty (Merritt & Milosavljević 2005). Since the binary must eject of order its own mass per e -folding in its semi-major axis, the system stops hardening around a_{hard} unless some other mechanism causes sufficient mass flux through the binary.

If the binary reaches a separation around

$$a_{\text{gw}} = 5.4 \times 10^{-2} \left(\frac{m_{\text{bin}}}{10^8 M_{\odot}} \right)^{3/4} \left[\frac{2q}{(1+q)^2} \right]^{1/4} \left(\frac{\tau_{\text{gw}}}{10^{10} \text{ yrs}} \right)^{1/4} f^{-1/4}(e) \text{ pc}, \quad (2)$$

where e is the orbital eccentricity of the binary and $f(e) = (1 - e^2)^{7/2} / (1 + 73e^2/24 + 37e^4/96)$, then it can coalesce on a timescale τ_{gw} through gravitational radiation (Begelman et al. 1980). To get from a_{hard} to a_{gw} it must bridge a gap

$$\frac{a_{\text{hard}}}{a_{\text{gw}}} \approx 29 \left(\frac{m_{\text{bin}}}{10^8 M_{\odot}} \right)^{-1/4} \left[\frac{2q}{(1+q)^2} \right]^{3/4} \quad (3)$$

by some mechanism other than stellar-dynamical friction or gravitational radiation. The question of whether and how it crosses this gap has become known as the “final parsec problem” (Merritt & Milosavljević 2005).

In many galaxies there probably are alternative mechanisms for crossing the gap. When gas-rich galaxies merge, tidal torques channel large amounts of gas into the central ~ 100 pc (Byrd et al. 1987; Hernquist 1989). The gas may lose energy through radiation and angular momentum through viscous torques, and is therefore not subject to a loss cone problem. Using Smoothed Particle Hydrodynamics simulations Escala et al. (2004, 2005) compute a merger time of order 10^7 yrs in an environment typical of the central regions of ULIRGs, which are thought to be gas-rich galaxies caught in the act of merging (Sanders et al. 1988). The nuclei of galaxies are also observed to contain numerous massive perturbers such as star clusters, molecular clouds, and possibly intermediate-mass black holes (IMBH). These objects scatter stars into the loss cone much more efficiently than other stellar mass objects, since the relaxation rate scales as the perturber mass for a fixed mass density of perturbers. Perets et al. (2006) extended the Fokker-Planck loss cone formalism to accommodate a spectrum of perturber masses and account for relaxation by rare close encounters with massive perturbers. They show that the population of known massive perturbers in the nucleus of the Milky Way is sufficient to bring a $4 \times 10^6 M_{\odot}$ BH binary to a_{gw} in $\sim 6 \times 10^8$ yrs, and it is reasonable to expect similar perturber populations in other star-forming spiral galaxies.

In addition to these alternative mechanisms, the stellar self-relaxation rate is probably at least a factor of a few higher than that predicted by standard loss-cone theory (Frank & Rees 1976; Lightman & Shapiro 1977; Cohn & Kulsrud 1978) in real galaxies. Higher-mass stars and stellar remnants tend to segregate toward the center, shortening the relaxation time by a factor of a few. Resonant relaxation caused by coherent torques between stars bound to the central SMBH may dominate over two-body relaxation by up to a factor of 10 in the center of our galaxy (Hopman & Alexander 2006). In addition the loss cone-clearing process itself enhances the two-body relaxation rate. When all stars with angular momenta below $L_{lc} \sim r\sigma\theta_{lc}$ are ejected, this creates a near step function in the angular momentum distribution. Since the diffusion coefficients are proportional to the phase space gradients, this sharp feature in angular momentum space can shorten the relaxation time significantly. The binary hardening time may be shorter than that computed assuming the standard equilibrium distribution function by up to a factor of ~ 10 , which is already sufficient to bring the loss cone refilling time below a Hubble time in many small galaxies with dense nuclei (Milosavljević & Merritt 2003).

The final parsec problem is often mentioned as a caveat when predicting the SMBH coalescence signal in low-

frequency gravitational wave detectors such as the upcoming Laser Interferometer Space Antenna (LISA). However the LISA event rate is expected to be dominated by small galaxies at high redshift (Wyithe & Loeb 2003a; Sesana et al. 2005; Rhook & Wyithe 2005), where the gas content and central densities tend to be high and the relaxation times short. For this reason *the stalling problem is probably not a significant concern for the LISA SMBH coalescence signal*. On the other hand BH ejections by gravitational radiation recoil (Merritt et al. 2004; Haiman 2004) may play an important role in the high-redshift coalescence rate. The long-term survival of SMBH binaries is likewise unlikely in the gas-rich cores of quasars and ULIRGs.

However none of the gap-crossing mechanisms discussed so far are likely to reduce the coalescence time below a Hubble time in mergers between giant, gas-poor elliptical galaxies. Merritt & Poon (2004) show that a significant fraction of stars on “centrophilic” orbits in a triaxial potential can greatly increase the mass flux into the loss cone. Such box orbits are often observed in the products of collisionless mergers in N-body simulations (Naab et al. 2006; Cox et al. 2006 and references therein) and in real elliptical galaxies (e.g. Kormendy & Bender 1996; Hao et al. 2006). Some non-axisymmetric potentials can also excite bar instabilities that cause rapid mass flow through the binary and efficient coalescence (Berczik et al. 2006). However a central SMBH can disrupt box orbits and induce axisymmetry in the inner regions of a triaxial galaxy (Merritt & Quinlan 1998; Holley-Bockelmann et al. 2002), and it is uncertain how often these geometry-specific mechanisms bring the coalescence time below a Hubble time.

One can naively assess the likelihood of coalescence by considering the “full” and “empty” loss cone hardening times, τ_{full} and τ_{empty} , in the nuclei of various galaxies assuming a spherical and isotropic distribution function. τ_{full} is the hardening time assuming every star kicked out of the loss cone is instantly replaced, while τ_{empty} is the time assuming stellar two-body relaxation to be the only replenishing mechanism. In small, dense galaxies $\tau_{full} \sim 10^{5-6}$ yrs and $\tau_{empty} \sim 10^{9-10}$ yrs while in the lowest-density cores of giant ellipticals and cD galaxies $\tau_{full} \sim 10^8$ yrs and $\tau_{empty} \sim 10^{14}$ yrs (Yu 2002). While the empty loss cone rate is difficult to believe in any galaxy given at least some clustering on scales larger than $1 M_\odot$, it also seems difficult to approach the full loss cone rate if there is no gas around and no strong radial bias in the stellar distribution. From this point of view the stalling of binaries seems unlikely in small galaxies but probable in low-density, gas-poor ellipticals.

At present there is no conclusive observational evidence either for or against the prevalence of (sub)parsec-scale SMBH binaries. These scales can only currently be resolved with VLBI at very low redshift, where the number of systems luminous enough to detect is expected to be small. The systems most likely to stall may also be the most difficult to observe, since the accretion processes that produce radiation are also conducive to binary coalescence. (Semi-)periodic temporal variations in AGN lightcurves and double-peaked broad emission lines have been taken as indirect evidence for sub-parsec scale binaries (Komossa 2003 and references therein). Perhaps the most convincing case is OJ 287 due to its (so far) strict optical periodicity of ~ 12 yrs (Sillanpää et al. 1988, 1996; Valtaoja et al. 2000;

Pursimo et al. 2000). If the interpretation of the flares in OJ 287 as a binary companion piercing the primary accretion disk twice per orbital period is correct, then the gravitational radiation time for this system is much shorter than a Hubble time. The direct binary interpretation of the double-peaked broad emission line profiles has been ruled out by various physical arguments (see Eracleous & Halpern 2003). Most of the profiles are well fit by circular relativistic accretion disk models. The rest ($\sim 30\%$) can be modelled as elliptical disks which could arise from tidal perturbations caused by a more distant binary companion (Eracleous et al. 1995). The binary hypothesis for the periodic lightcurves would be strongly favored by observations of different time variations at different wavelengths, presumably emanating from different parts of the accretion flow (Hayasaki et al. 2006; Rieger 2006). X-shaped radio jets have been interpreted in terms of spin flips that occur when two SMBH coalesce (Merritt & Ekers 2002), and helical deformations in such jets have also been attributed to SMBH binaries (e.g. Begelman et al. 1980; Roos et al. 1993). The shallow cores of massive elliptical galaxies are thought to be fossil relics of the heating and stellar mass ejection caused by inspiralling binary SMBH that either stall or coalesce (Milosavljevic & Merritt 2001).

If some binaries do survive for around a Hubble time, then the hierarchical buildup of galaxies will inevitably place three or more SMBH in some merging systems.

1.2 Merger-induced binary evolution before three-body interactions: Back-of-the-envelope calculations

An inspiralling satellite affects the evolution of a binary SMBH, even long before it sinks to the center, by perturbing the large-scale potential and scattering stars into the loss cone. We may estimate the extent of this effect as a function of satellite mass and distance from the center of the host galaxy using a rough but simple argument due to Roos (1981). The change in velocity necessary to deflect a star at radius q into the loss cone is $\Delta V \sim h_{lc}/q$, where $h_{lc} \sim \sigma \sqrt{r_{inf} r_{bin}}$ is the characteristic specific angular momentum of stars on loss cone orbits (Frank & Rees 1976), $r_{inf} = Gm_{bin}/\sigma^2$ is the SMBHs’ radius of influence, and r_{bin} is the binary separation. The dynamical time at this radius is $t_{dyn} \sim q/\sigma$, so the acceleration required to scatter a star into the loss cone is roughly $a_{lc}(q) \sim \Delta V/t_{dyn} \sim \sigma^2 \sqrt{r_{inf} r_{bin}}/q^2$. Equating this with the tidal acceleration caused by the satellite, $a_{tid} = 2GM_{sat}(r)q/r^3$, where r is the satellite’s radius, yields $q^3 = \sigma^2 \sqrt{r_{inf} r_{bin}} r^3 / 2GM_{sat}(r)$, or with $r_{bin} = a_{hard} = G\mu/4\sigma^2$,

$$q = \left[\frac{\sqrt{m_{bin}\mu}}{4M_{sat}(r)} \right]^{1/3} r. \quad (4)$$

The r -dependence of M_{sat} reflects the tidal stripping of the satellite as it spirals inward. Equation (4) defines a critical radius q , outside of which the satellite can deflect stars into (and out of) the loss cone in one dynamical time. The mass flux through the binary induced by the satellite is then approximately

$$\frac{dM_{stars}}{dt}(q) = 2\pi\rho(q)q^2\sigma\theta_{lc}^2, \quad (5)$$

where $\rho(q)$ is the density of the host galaxy at radius q and $\theta_{lc}^2 \approx r_{inf} r_{bin} / r^2$ is the geometrical factor accounting for the fraction of stars on loss cone orbits as a function of radius r , assuming an isotropic distribution function (Frank & Rees 1976). For a fixed satellite mass and distance, we can then define a “binary feeding” timescale by

$$\tau_{feed} = \frac{m_{bin}}{dM_{stars}/dt} = \frac{m_{bin}}{2\pi\rho(q)q^2\sigma\theta_{lc}^2(q)}. \quad (6)$$

To determine whether the scattering of stars into the loss cone by the satellite is sufficient to harden the binary enough to prevent a close three-body encounter before the intruder arrives at the galactic center, we must compare τ_{feed} with the timescale on which the satellite spirals in by dynamical friction. In the approximation of slow inspiral we may write the dynamical friction timescale as $\tau_{df} \equiv |r/\dot{r}| \approx |v/(dv/dt)|_{df}$. Substituting $(dv/dt)_{df}$ from Chandrasekhar’s formula (equation (28) in §2.4; Chandrasekhar 1943) yields

$$\tau_{df}(r) = \frac{v_{sat}^3(r)}{4\pi\rho(r)M_{sat}(r)[\text{erf}(X) - \frac{2X}{\sqrt{\pi}}e^{-X^2}]}, \quad (7)$$

where $X \equiv v_{sat}/\sqrt{2}\sigma$. $v_{sat}(r)$ in equation (7) is computed from $v_{sat}(r) = \sqrt{GM_{host}(r)/r}$, where $M_{host}(r) = M_{stars}(r) + M_{halo}(r) + m_{bin}$ is the mass of the host galaxy enclosed within radius r . $M_{sat}(r)$ is the satellite mass contained within the tidal truncation radius obtained from a simple point mass approximation, $r_{tid} = [M_{sat}/M_{host}]^{1/3}r$ (this slightly underestimates r_{tid} as the satellite approaches the center of the host). In Fig. 1 we plot τ_{df} and τ_{feed} as a function of r for a satellite with one third the stellar mass of the host, which contains a binary with $(m_1, m_2) = (1.2, 3.7) \times 10^8 M_\odot$. Both host and satellite are modelled as Hernquist profiles (Hernquist 1990), with their masses and effective radii set by observed scaling relations. The details of the galactic model are described further in §2.

Since τ_{feed} remains about an order of magnitude above τ_{df} throughout the inspiral, this simple calculation makes it plausible that the binary survives the merger process and undergoes close triple interactions with the infalling SMBH. The tidal approximation (as well as our treatment of dynamical friction) breaks down as the satellite approaches r_{inf} , so the plot is cut off at a separation of ~ 100 pc, when the satellite still has ~ 4 e -foldings to go to reach a_{hard} . However this final stage of the inspiral is found to proceed very rapidly in N-body simulations (Quinlan & Hernquist 1997; Milosavljevic & Merritt 2001; Merritt 2006). The merger’s effect on the binary may be dominated by violent relaxation or collective effects such as a bar instability (Berczik et al. 2006), in which case our two-body approach does not capture its essence. The evolution of the core distribution function under the influence of a major merger is an intriguing open problem for simulators.

After the third BH becomes bound to the binary (but still before the onset of close three-body interactions) another hardening mechanism may become important. If the angle of inclination i of the outer binary (formed by the intruder and the inner binary center-of-mass) exceeds a critical angle $\theta_{crit} \approx 39^\circ$, then the quadrupolar perturbation from the intruder induces eccentricity oscillations through a maximum (Kozai 1962)

$$e_{max} \approx \sqrt{1 - \frac{5}{3}\cos^2 i}. \quad (8)$$

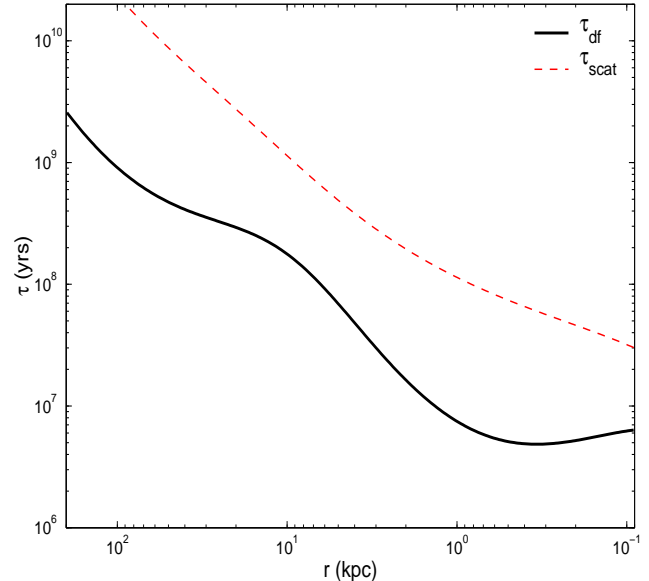


Figure 1. Comparison of the “feeding timescale”, τ_{feed} , on which an inspiralling satellite scatters mass into the loss cone of an SMBH binary, with the dynamical friction timescale, τ_{df} , on which the satellite spirals in. Upper (red dashed) line: τ_{feed} computed from equation (6); Lower curve: τ_{df} computed from equation (7). Both timescales are plotted as a function of the satellite’s distance from the center of the host galaxy. For this plot we chose a binary mass of $4.5 \times 10^8 M_\odot$ and merger mass ratio of 3:1 in the stars. The galactic model is discussed in the text.

Since the gravitational radiation rate increases sharply toward high eccentricities, these “Kozai oscillations” can greatly enhance the radiation, possibly causing the binary to coalesce before it can undergo strong three-body interactions with the intruder (Blaes et al. 2002). General relativistic precession can destroy the Kozai resonance (e.g. Holman et al. 1997), but Blaes et al. (2002) find that this does not happen for

$$\frac{a_{out}}{a_{in}} \lesssim 43 \left[2q_{out} \left(\frac{a_{in}}{1 \text{ pc}} \right) \left(\frac{10^8 M_\odot}{m_{bin}} \right) \right]^{1/3} \sqrt{\frac{1 - e_{in}^2}{1 - e_{out}^2}}, \quad (9)$$

where a_{in} and a_{out} are the semi-major axes of the inner and outer binaries, q_{out} is the outer binary mass ratio, and e_{in} and e_{out} are the inner and outer eccentricities. This leaves a window of about a factor of 10 in a_{out}/a_{in} in which the Kozai mechanism can operate before unstable three-body interactions begin.

The actual enhancement of the gravitational radiation rate of course depends on the amount of time spent at high eccentricity, but one may place an upper limit on the importance of Kozai oscillations by computing the radiation timescale if the inner binary spends all of its time at e_{max} . The orbit-averaged power radiated by gravitational radiation is given by

$$\left| \frac{dE}{dt} \right|_{gw} = \frac{32G^4 m_1^2 m_2^2 (m_1 + m_2)}{5c^5 a^5} \frac{1 + \frac{73}{24}e^2 + \frac{37}{96}e^4}{(1 - e^2)^{7/2}} \quad (10)$$

(Peters 1964), where a is the semi-major axis and e is the eccentricity. In Fig. 2 we plot contours of the gravitational radiation time $\tau_{gw} = |E/(dE/dt)|_{gw}$ in the a - i plane by putting e_{max} into equation (10), for an equal-mass $6 \times 10^8 M_\odot$ binary. This may seem like a gross overestimate of the

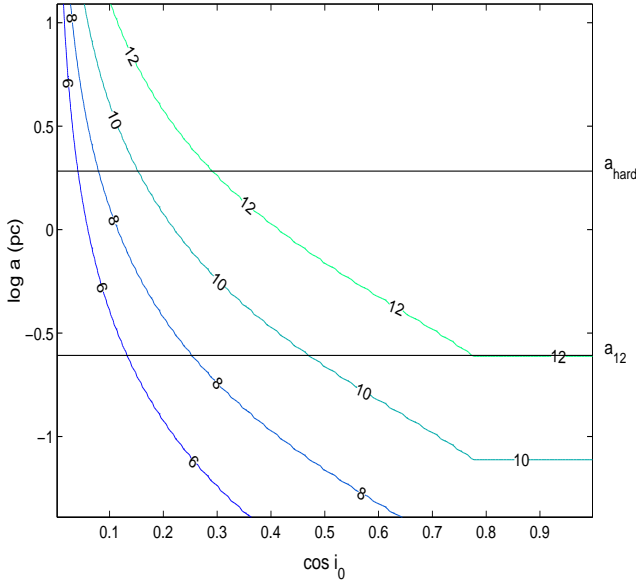


Figure 2. Upper limit on the importance of Kozai oscillations in enhancing gravitational radiation by the inner binary ($m_1 = m_2 = 3 \times 10^8 M_\odot$). The cosine of the initial inclination angle is plotted on the horizontal axis, and the inner binary semi-major axis is plotted on the vertical axis. Contours are plotted for gravitational radiation timescales of $\tau_{gw} = 10^{12}, 10^{10}, 10^8$, and 10^6 yrs, if the binary were to stay at maximum eccentricity throughout the whole oscillation cycle. The horizontal lines indicate the hardening radius and the separation such that a circular binary would coalesce on a 10^{12} yr timescale.

gravitational radiation rate, especially since the shape of the Kozai oscillations is in fact such that the binary spends more time near e_{min} than near e_{max} . However since τ_{gw} is so strongly dominated by pericenter passages at $e \approx e_{max}$, the shift in the contours for a realistic high- e duty cycle is only modest. See (Blaes et al. 2002) for comparison with a detailed study of radiation enhancement by Kozai oscillations in binaries with initial $\tau_{gw} \sim 10^{12}$ yrs. For a binary at a_{hard} , Kozai oscillations can induce coalescence within 10^{10} yrs in $\lesssim 20\%$ of cases assuming $\cos i$ is uniformly distributed. In the remainder of cases the inner binary may survive until the outer binary shrinks to the point of unstable three-body interactions.

1.3 Close three-body encounters

If dynamical friction brings the intruder close enough before the perturbation causes sufficient hardening of the (inner) binary, then a strong three-body encounter takes place. Strong encounters are characterized by a significant transfer of energy between the binary's internal degrees of freedom and the center-of-mass motion of the binary and third body. When the intruder is slow relative to the binary's orbital speed v_{bin} , energy typically flows from the inner binary to the outer components, so that the binary is more strongly bound after the encounter. This is one manifestation of the negative specific heat characteristic of gravitationally bound systems. The encounter ends in the escape of one of the three bodies, usually the lightest, from the system at a speed comparable to v_{bin} .

When the lightest body m_3 escapes, momentum conservation requires that the binary (m_1, m_2) center-of-mass recoil in the opposite direction with a speed smaller by a factor $m_3/(m_1 + m_2)$. It is instructive to compare the expected ejection velocities of the binary and escaper with the typical galactic escape velocity. For a circular binary with $m_1 = m_2 = m_{bin}/2$, the binding energy at the hardening radius is $E_{B,hard} = Gm_{bin}^2/8a_{hard} \approx 6.8 \times 10^{55} [m_{bin}/(10^8 M_\odot)]^{3/2}$ erg. The binding energy at the radius where $\tau_{gw} = 10^8$ yrs is $E_{B,gw} = Gm_{bin}^2/8a_{gw} \approx 6.2 \times 10^{57} [m_{bin}/(10^8 M_\odot)]^{5/4}$ erg. The mean energy ΔE harvested from the binary in close encounters with slow intruders is about $0.4E_B$, though the median ΔE is somewhat lower (Hills & Fullerton 1980). Energy conservation implies that the escaper leaves the system with kinetic energy $KE_{sing} = \Delta E/[1+m_3/(m_1+m_2)]$ while the binary leaves with $KE_{bin,cm} = \Delta E/[1+(m_1+m_2)/m_3]$ in the system center-of-mass frame. For an equal mass binary with $m_{bin} = 5 \times 10^8 M_\odot$, this gives ejection velocities of $v_{sing} \sim 290$ km/s and $v_{bin} \sim 140$ km/s for the binary at a_{hard} , and $v_{sing} \sim 4000$ km/s and $v_{bin} \sim 2000$ km/s for the binary at a_{gw} .

Any nonzero eccentricity of the binary will increase the semi-major axis corresponding to a fixed τ_{gw} , lowering the ejection velocities for the binary at a_{gw} . Also any deviation from equal masses (the chance of all three masses being very nearly equal in a real galaxy is small) will result in a smaller fraction of the extracted energy being apportioned to the binary and a smaller binary recoil velocity. The typical escape velocity for galaxies hosting $5 \times 10^8 M_\odot$ BHs is around 1500 km/s, accounting for both the stars and the dark matter. From these numbers, it appears that single escapes will be fairly common as repeated encounters harden the binary to $\sim a_{gw}$. However accounting for realistic mass ratios and eccentricities (recall that the first three-body encounter thermalizes the eccentricity even if it starts off circular), binary escapes should be rare. Since the binary must come near the escape velocity to remain outside the nucleus for a significant amount of time, we do not expect triple interactions to empty many nuclei of BHs. We will quantify these statements with our triple-BH simulations.

The formation of triple SMBH systems through inspiral of a merging satellite leads to a rather specific initial configuration. Unlike in most numerical three-body scattering experiments (e.g. Hut & Bahcall 1983), the three BHs start off as a bound “hierarchical triple.” A triple system is called hierarchical if the outer binary is much more widely separated than the inner binary, $a_{out}/a_{in} \gg 1$. In studies like Hut & Bahcall (1983) the encounters are traditionally sorted into three categories: (i) “flybys” in which the intruder just passes through, exchanging some energy and angular momentum with the binary along the way; (ii) “exchanges” in which the intruder trades places with one of the binary members and a different body escapes; and (iii) “resonant encounters” in which the three bodies become temporarily bound before one of them escapes. Encounters of type (iii) can last for hundreds or even thousands of dynamical times and are by far the most complex and computationally expensive. However the hierarchical triple initial conditions given by the merger formation route put every encounter in category (iii), making a precise but efficient integrator essential for a project aimed at studying SMBH triples in galactic nuclei.

For very large a_{out}/a_{in} we expect hierarchical triples to exhibit very regular behavior; in this case the third body sees the inner binary as a point mass and the system essentially consists of two independent (inner and outer) binaries. However as a_{out}/a_{in} approaches unity, secular evolution gives way to chaotic three-body interactions in which the orbits diverge and the system becomes subject to escape of one its components. Mardling & Aarseth (2001) derive a criterion for the stability of three-body systems based on an analogue with the problem of binary tides. The most distant intruder orbit at which unstable interactions can begin is reliably estimated by

$$\frac{R_p^{out}}{a_{in}} \approx 2.8 \left[\frac{(1 + q_{out})(1 + e_{out})}{\sqrt{1 - e_{out}}} \right]^{2/5}, \quad (11)$$

where R_p^{out} is the pericentre separation of the outer binary, a_{in} is the semimajor axis of the inner binary, $q_{out} = m_3/(m_1 + m_2)$ is the outer binary mass ratio, and e_{out} is its eccentricity. This criterion has great practical importance due to the high numerical cost of unnecessarily following weak hierarchical systems. It specifies an optimal starting point for our simulations, which aim to study strong interactions in three-body systems starting off as hierarchical triples.

Naively one might expect a strong three-body encounter following a merger with a galaxy hosting a binary, so long as the intruder does not induce coalescence of the binary before it reaches the center. However the stability criterion implies a condition for close interactions much more stringent than this. To undergo a chaotic encounter with the inner binary, the intruder must reach the stability boundary before the outer binary hardens and stalls. A triple system covers somewhat more stellar phase space than a binary of the same size, but not by much for a stable hierarchical system. This means that the merger process cannot cause the binary to harden by more than around an e -folding for a nearly circular, equal-mass system before the intruder arrives at the center. Though the order-of-magnitude estimates in the previous section make this plausible, further study is needed to determine the likelihood of unstable triple interactions in realistic merger situations. An eccentric outer binary relaxes the criterion somewhat, but dynamical friction tends to circularize the orbits of satellites with moderate initial eccentricities before they reach the nucleus (Milosavljević & Merritt 2001). We therefore assume near-circular initial orbits and begin each simulation from a weakly hierarchical configuration.

1.4 Motivation for this work

The problem of binary or multiple SMBH systems in galactic nuclei is not very amenable to “brute force” simulation. Since the two-body relaxation time scales as the number of bodies N , stellar relaxation proceeds much faster in simulations where one particle represents $\sim 10^{4-7}$ stars than in real galaxies. A simulation with $M_{stars}/m_{bh} \sim 10^3$ requires $\sim 10^8$ particles to be in the “empty loss cone” regime where the timescale for diffusion into the loss cone far exceeds the core dynamical time. Since general relativistic effects become important during close encounters between BHs, the problem demands high-precision integration of the BH trajectories in full post-Newtonian gravity. Star-BH interactions pose the numerical challenge of accurately treat-

ing close encounters between pairs with extreme mass ratios. Since stellar relaxation may be significantly enhanced by massive perturbers such as star clusters (Perets et al. 2006), the simulations must employ realistic models of the clumpiness of galaxies. The time-varying, asymmetric potential arising from the merger process may also play an important role in the fate of the BH system. Hence ideally the BH orbits must be computed within a galaxy merger simulation, which resolves the stellar cusps around the BHs and is not dominated by spurious relaxation. It is unlikely that simulations will meet all of these demands anytime in the near future.

However a range of clever methods have been used to quantify many aspects of the SMBH binary problem (see Merritt & Milosavljević 2005 for an excellent review). For instance Quinlan & Hernquist (1997) simulated SMBH binary evolution in the collisionless regime by treating BH-BH and BH-star interactions as a $1/r^2$ force between pairs, but deriving the force on a star due to other stars from a smoothed potential. They suppressed exaggerated Brownian wandering of the BHs (Chatterjee et al. 2003) by subtracting off the center-of-mass force on the binary at each timestep. Milosavljević & Merritt (2003) iteratively solved the time-dependent Fokker-Planck equation for diffusion of stellar orbits in angular momentum space to obtain fluxes into the loss cone up to ten times higher than those computed using the standard quasi-steady state loss cone theory (Frank & Rees 1976; Lightman & Shapiro 1977; Cohn & Kulsrud 1978). Merritt (2006) performed N-body simulations of successive galactic mergers to study the cumulative flattening of the cores by the inspiralling SMBHs. Though his simulations were in the full loss cone regime, he identified the stalling radius with the point where the binary began hardening at a constant rate ($dE/dt = \text{const}$). From these and other studies we have learned a good deal about the properties of SMBH binaries under many circumstances - e.g. their hardening rates, characteristic radii and eccentricities, and effect on the surrounding stars and dark matter.

Less work has been devoted to the problem of multiple-SMBH systems in galactic nuclei. Valtonen et al. (1994) performed an extensive series of three- and four-body scattering experiments in a Plummer model galactic potential, with a friction force used to represent gravitational radiation. They compared their ejection statistics with observed single- and double-sided lobes in extended radio sources, exploring the possibility that the lobes could result from slingshot ejections of BHs. However since enormous progress has been made in our understanding of the inner density profiles of galaxies, SMBH/stellar bulge correlations, galaxy merger rates, and the fate of satellite galaxies since this study, their initial conditions are rather arbitrary in light of our current knowledge. They also made no attempt to model stellar hardening of the binary, and since they did not regularize the equations of motion, many runs involving long-lived hierarchical resonances had to be thrown out. Iwasawa et al. (2005) performed the first full N-body simulations of equal-mass triple BH systems embedded in stellar bulges, an important contribution to our understanding of galactic nuclei. Because of the large computation time required for each run, they could not statistically sample the highly varied outcomes of the three-body encounters as Valtonen et al.

(1994) did. Since their highest-resolution simulations used only $\sim 10^5$ particles for reasons of computational efficiency, any relevant loss cone effects may have been lost to spurious relaxation.

In this paper we study the outcomes of triple SMBH interactions in galactic nuclei using physically-motivated initial BH configurations, BH mass distributions, and galactic models characteristic of the low-density, massive elliptical galaxies in which SMBH binaries are most likely stall. We follow the BH trajectories during close three-body encounters using a KS-regularized Bulirsch-Stoer integrator provided by Sverre Aarseth (Mikkola & Aarseth 1990, 1993). We do not treat star-BH interactions individually, but instead model the collective effect of the stars on the BH orbits using a simple analytic prescription. The inner density profile is updated throughout our simulations to roughly account for core heating by dynamical friction and stellar mass ejection. Gravitational radiation losses are modelled as a drag force dependent on the relative coordinates of each pair. The simulation ends when the time since the last merger has elapsed or a stationary state is reached: only one SMBH remains in the galaxy and it has settled to rest at the center, two BHs remain and have formed a stalled binary, or all BHs have escaped the galaxy. Each simulation takes only a few minutes to run on a single processor, so we can try a variety of distributions of initial conditions and statistically sample the outcomes for each.

Aside from the motivating order-of-magnitude calculations in previous sections, this paper does not address the question of *whether* close triple SMBH systems form in galactic nuclei. We start our simulations from a state that the system must reach shortly before the onset of unstable three-body interactions *assuming* that they occur, and proceed to derive the subsequent evolution. Our results may be used to argue for or against the occurrence of triple systems in real galaxies, as observations support or disfavor the signatures that we derive.

In section 2 we describe our model and code methods. In section 3 we present the results of our study: the outcome statistics, predicted semi-major axis and eccentricity distribution of observed binaries if three-body interactions are prevalent, the efficiency of coalescence induced by the encounters, the ejection statistics and typical distances of closest approach, and the extent of the core scouring caused by the triple SMBH systems. In section 4 we discuss these results and conclude.

2 MODEL AND METHODS

2.1 BH mass distribution and halo model

To get a physically motivated distribution of BH mass ratios, we associate the formation of the inner and outer binaries with the last two major mergers in the history of the galactic halo hosting the triple system. We use Extended Press-Schechter (EPS) theory (Lacey & Cole 1993) to calculate the probability distributions of the halo formation times and progenitor masses, and randomly select the parameters of the previous two mergers from these distributions. We then assign a BH to each progenitor halo using a simple prescription based on the assumption of a flat galactic rotation curve.

Press & Schechter (1974) derived a useful analytic expression for the number density of halos in the universe as a function of mass and redshift, $N(M, z)$, by assuming a Gaussian random field of primordial density fluctuations and associating bound objects with volumes whose average over-densities have crossed the threshold $\delta_c \approx 1.69$ for gravitational collapse in their linear growth. Bond et al. (1991) provided a more careful derivation of the expression obtained by Press & Schechter, based on the rate of diffusion of the over-density across the threshold δ_c as k progresses from larger to smaller scales. In the process they obtained the conditional density $\tilde{N}(M_1, z_1)$ of objects that will be incorporated into larger objects of mass M_2 at later time z_2 . By taking the limit $z_2 \rightarrow z_1$, Lacey & Cole (1993) used this formulation to derive an instantaneous merger rate,

$$r_{LC}(M_1, M_f, t) = \frac{d^2 p}{dM_2 dt} = \sqrt{\frac{2}{\pi}} \frac{\delta_c}{D(z)} \left| \frac{\dot{\delta}_c}{\delta_c} - \frac{\dot{D}}{D} \right| \cdot \frac{|d\sigma/dM|_{M_f}}{\sigma^2(M_f)} \frac{\exp \left[-\frac{\delta_c^2}{2D^2(z)} \left(\frac{1}{\sigma^2(M_f)} - \frac{1}{\sigma^2(M_1)} \right) \right]}{[1 - \sigma^2(M_f)/\sigma^2(M_1)]^{3/2}}. \quad (12)$$

This equation gives the probability, per unit time per unit mass of M_2 , of a given halo of mass M_1 merging with another halo of mass M_2 to form a product of mass $M_f = M_1 + M_2$ at time t . Here $\sigma^2(M)$ is the present-day variance of the linear density field on mass scale M ,

$$\sigma^2(M) = \frac{1}{(2\pi)^3} \int_0^\infty P(k) W^2(kr) 4\pi k^2 dk, \quad (13)$$

where $P(k)$ is the power spectrum of density fluctuations today, W is a tophat window function, and r is related to M through $M = (4/3)\pi r^3 \rho_m$, the volume times the present-day matter density. $P(k)$ is related to the primordial power spectrum through the transfer function $T(k)$, which encapsulates the suppression of perturbations on small scales due to radiation pressure and damping over the history of the universe. For $T(k)$ we adopt the standard fitting formulae of Eisenstein & Hu (1998). For the linear growth function $D(z)$ we use the approximation

$$D(z) \approx \frac{(5/2) \Omega_m(z)}{\Omega_m^{4/7}(z) - \Omega_\Lambda(z) + \left[1 + \frac{\Omega_m(z)}{2} \right] \left[1 + \frac{\Omega_\Lambda(z)}{70} \right]}, \quad (14)$$

which is good to within a few percent for all plausible values of Ω_m and Ω_Λ (Carroll et al. 1992). $\Omega_m(z) = \Omega_m(1+z)^3 / [\Omega_m(1+z)^3 + \Omega_\Lambda]$ is the matter density (normalized to the critical density) as a function of redshift and we take $\Omega_\Lambda(z) = 1 - \Omega_m(z)$ assuming the rest of the density is in the form of a cosmological constant. δ_c has the weak redshift dependence (Kitayama & Suto 1996)

$$\delta_c \approx \frac{3(12\pi)^{2/3}}{20} [1 + 0.0123 \log_{10} \Omega_m(z)]. \quad (15)$$

We adopt the cosmological parameters obtained from three years of data collection by the Wilkinson Microwave Anisotropy Probe (WMAP), $\Omega_m h^2 = 0.127$, $\Omega_b h^2 = 0.0223$, $h = 0.73$, $\sigma_8 = 0.74$, and $n_s = 0.951$ (Spergel et al. 2006).

Since the merger rate (12) diverges as $M_2/M_1 \rightarrow 0$, applications of the formula that track individual merging halos must employ a cutoff mass ratio $M_2/M_1 \equiv \Delta_m$, such that all mergers below Δ_m are treated as smooth *accretion* rather than as discrete mergers (see Manrique & Salvador-Sole 1996 for further discussion). The instantaneous rate of ac-

cretion onto a halo of mass M at redshift z is

$$r_a(M, t) = \int_M^{M(1+\Delta_m)} (M' - M) r_{LC}(M, M', t) dM'. \quad (16)$$

To get the growth history (“accretion track”) of a halo of mass M_0 at time t_0 due to accretion since the last merger, one need only solve the differential equation $dM/dt = r_a[M(t), t]$, subject to the initial condition $M(t_0) = M_0$. We integrate this equation backward in time using a 4th-order Runge-Kutta method to get the accretion tracks of the halos in our simulations. Since we are interested in BH binary formation, we loosely associate Δ_m with the halo mass ratio such that tidal stripping of the satellite would prevent the eventual merging of the two nuclei. N-body simulations of galaxy mergers place this mass ratio in the range $\Delta_m \sim 0.1 - 0.3$, depending on the density and orbital parameters of the satellite (Taffoni et al. 2003; Colpi et al. 1999). Hence our canonical choice is $\Delta_m = 0.3$, and we also try values of $\Delta_m = 0.1$ (runs D1) and 0.5 (runs D5), the latter being the halo mass that corresponds to a stellar mass ratio of $\sim 3:1$ in our prescription.

Following Salvador-Sole, Solanes, & Manrique (1998), we write the probability, per unit time, of a halo with mass M_f at time t arising from a merger with a smaller halo of mass between M and $M + dM$ (the “capture rate”) as

$$r_c(M, M_f, t) dM = r_{LC}(M, M_f, t) \theta[M_f - M(1 + \Delta_m)] \frac{N(M, t)}{N(M_f, t)} dM, \quad (17)$$

the EPS merger rate excluding halos below the threshold Δ_m , and weighted by the number of mass M halos per unit halo of mass M_f . Equation (12) gives the probability of a *given* halo of mass M merging to form a halo with final mass M_f , whereas here we want the rate at which mass M_f halos are created out of *all* progenitors of mass M .

The rate at which halos of mass M_f form through all mergers at time t is

$$r_f(M_f, t) = \frac{1}{2} \int_{M_f \Delta_m / (1 + \Delta_m)}^{M_f} r_c(M, M_f, t) dM, \quad (18)$$

employing the approximate symmetry of $r_c(M, M_f, t)$ about $M_f/2$ on the range $M_f \Delta_m / (1 + \Delta_m) < M < M_f / (1 + \Delta_m)$ (see Fig. 1 of Raig, Gonzalez-Casado, & Salvador-Sole 2001). The probability distribution function (PDF) of formation times of halos with mass M_0 at time t_0 is

$$\Phi_f(M_0, t) = r_f[M(t), t] e^{-\int_{t_0}^{t_f} r_f[M(t'), t'] dt'}. \quad (19)$$

Given a formation time t_f and corresponding mass $M(t_f)$ along the past accretion track of M_0 , the mass of the larger progenitor M_1 is distributed according to

$$\Phi_p[M(t_f), M_1] = \frac{2G(M_1, M)}{\int_{M \Delta_m / (1 + \Delta_m)}^{M / (1 + \Delta_m)} G(M', M) dM'}, \quad (20)$$

where

$$G(M', M) = \frac{|d\sigma(M')/dM'|}{M' \sigma^2(M')} \left[1 - \frac{\sigma^2(M)}{\sigma^2(M')} \right]^{-3/2}. \quad (21)$$

By choosing formation times and progenitor masses randomly according to (19) and (20), we capture the stochasticity of the intervals between mergers above Δ_m , but treat merging below this threshold only in the mean. See Raig, Gonzalez-Casado, & Salvador-Sole (2001), Salvador-Sole, Solanes, & Manrique (1998), and Manrique & Salvador-Sole (1996) for further details and

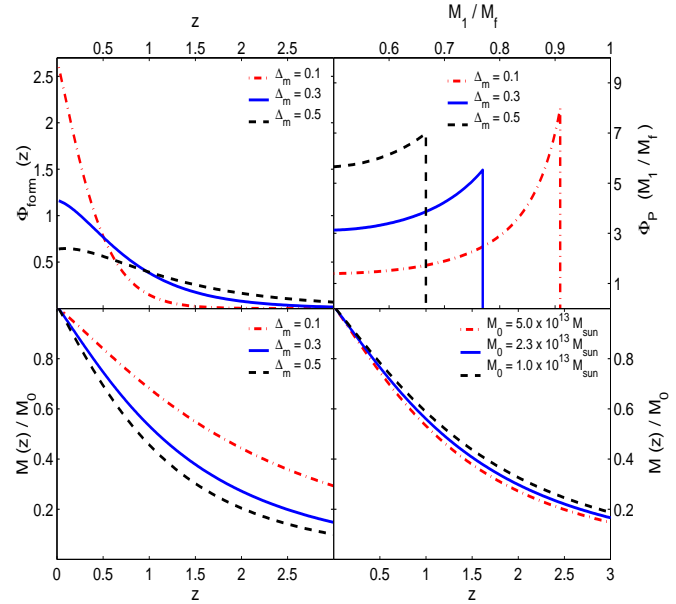


Figure 3. Upper left: Probability distribution function (PDF) of formation redshifts given by equation (19) for a $5 \times 10^{13} M_\odot$ halo at $z = 0$. Upper right: PDF of masses of the larger progenitor of the same halo given by equation (20), normalized to the mass of the merger product, $M_f = 5 \times 10^{13} M_\odot$. Lower left: Past accretion tracks of a present-day $5 \times 10^{13} M_\odot$ halo back to $z = 3$, normalized to the mass at $z = 0$. Lower right: Normalized accretion tracks for three different halo masses.

derivations of (19) and (20). Fig. 3 shows the distribution of formation times, progenitor masses, and accretion tracks for a present-day $5 \times 10^{13} M_\odot$ halo for $\Delta_m = 0.1, 0.3$, and 0.5, and the accretion tracks for 1, 2.3, and $5 \times 10^{13} M_\odot$ halos with Δ_m fixed at 0.3. All accretion tracks are normalized to the present-day mass M_0 . Note the insensitivity of the shape of these tracks to M_0 , as expected for masses above the critical mass $M^* \sim 2 \times 10^{12} M_\odot$.

Our algorithm for generating the BH masses is illustrated schematically in Fig. 4. For each run we begin with a halo of mass $M_0 = 5 \times 10^{13} M_\odot$ at time $t_0 \equiv t(z=0)$, choose its formation time t_{f0} randomly according to equation (19), and find the mass $M_{f0} = M(t_{f0})$ along its accretion track at that time. The mass M_{f0} is assigned to the dark matter halo hosting the triple BH system, and the physical time for the run to end if other termination conditions are not met first is set to $t_0 - t_{f0}$. To explore the dependence of the results on the absolute mass scale, we also try beginning with a $1 \times 10^{13} M_\odot$ halo (runs H1).

We model the halo as a Hernquist profile (Hernquist 1990), which is identical to an NFW profile (Navarro et al. 1997) in its inner regions if the scale radius a_H is related to the NFW scale radius by $a_H = a_{NFW} \sqrt{2[\log(1+c) - c/(1+c)]}$, where c is the halo concentration defined by $a_{NFW} = r_{vir}/c$. The Hernquist model falls off as r^{-4} instead of r^{-3} far outside a_H (Springel et al. 2005). The virial radius $r_{vir}(M, z)$ is given by

$$r_{vir}(M, z) = \frac{364}{1+z} \left[\frac{M_{halo}}{10^{13} h^{-1} M_\odot} \frac{\Omega_m(z)}{\Omega_m} \frac{18\pi^2}{\Delta_c} \right]^{1/3} h^{-1} \text{kpc}, \quad (22)$$

where $\Delta_c = 18\pi^2 + 82[\Omega_m(z) - 1] - 39[\Omega_m(z) - 1]^2$ (Barkana & Loeb 2001), and c roughly follows the median relation from the Λ CDM simulations of Bullock et al. (2001), $c \approx 9.0[(2.1 \times 10^{13} M_\odot)/M_{halo}]^{0.13}/(1+z)$. The z dependence of r_{vir} and c nearly cancel to make a_H depend only weakly on redshift, so we simply use the $z = 0$ relation between M_{halo} and a_H in our simulations.

We choose the mass M_1 of the larger progenitor of M_{f0} randomly according to equation (20), and assign a mass $M_2 = M_{f0} - M_1$ to the smaller progenitor. Before the merger the larger progenitor is assumed to have hosted a BH binary, while the smaller one hosted a single BH. Repeating the procedure used for M_0 , we assign formation times t_{f1} and t_{f2} to M_1 and M_2 using equation (19), and progenitor masses M_{11} , M_{12} , M_{21} , and M_{22} by equation (20).

Having constructed a set of progenitor halos, we now need a BH-halo relation $m_{bh}(M_{halo}, z)$ to complete our algorithm. We obtain such a relation by equating the halo virial velocity v_{vir} to the circular velocity v_c of the stellar spheroid, and using empirical $v_c - \sigma$ and $\sigma - m_{bh}$ correlations to connect v_c to m_{bh} , similar to the approaches in Erickcek et al. (2006) and Wyithe & Loeb (2005). Combining

$$v_{vir} = 343 \times \left(\frac{M_{halo}}{10^{13} h^{-1} M_\odot} \right)^{1/3} (1+z)^{1/2} \left[\frac{\Omega_m}{\Omega_m(z)} \frac{\Delta_c}{18\pi^2} \right]^{1/6} \text{ km s}^{-1} \quad (23)$$

(Barkana & Loeb 2001) with $v_c \approx 314[\sigma/(208 \text{ km/s})]^{0.84}$ km/s (Ferrarese 2002) and $\sigma/(208 \text{ km/s}) \approx [m_{bh}/(1.56 \times 10^8 M_\odot)]^{1/4.02}$ (Tremaine et al. 2002), we arrive at the relation

$$\left(\frac{M_{halo}}{10^{12} M_\odot} \right) = 8.28 \left(\frac{M_{bh}}{10^8 M_\odot} \right)^{0.626} \gamma(z), \quad (24)$$

where $\gamma(z) \equiv (1+z)^{-3/2}[(\Omega_m/\Omega_m(z))(\Delta_c/18\pi^2)]^{-1/2}$.

In our canonical runs we set the masses of the inner binary members to $m_{bh}(M_{11}, z_{f1})$ and $m_{bh}(M_{12}, z_{f1})$, and that of the intruding BH to $m_{bh}(M_{21} + M_{22}, z_{f2})$. Note that in this prescription the intruder is usually lighter than the heavier binary member, so that most of the three-body interactions result in an exchange. To examine the effect of more interactions without exchange, we try choosing $m_{bh}[\max(M_{21}, M_{22}), z_{f2}]$ for the intruder mass in runs (MX). As there is neither a direct causal relationship between m_{bh} and M_{halo} predicted by theory (Wyithe & Loeb 2005) nor a tight correlation directly observed between these two variables, and we know that identical halos may host galaxies of different morphologies and occupation numbers, $m_{bh}(M_{halo}, z)$ should be taken with something of a grain of salt. Nevertheless it is a useful way to generate simple but physically-motivated BH mass distributions when no information other than the halo mass is available.

We make one final modification to the set of BH masses used in our simulations. If the outer binary's hardening radius lies outside the stability boundary given by equation (11) with $a_{in} = a_{hard}$, then the decay of the outer orbit is expected to stall before a strong encounter can begin. To roughly account for this we exclude all initial conditions where $\mu_{out} > 3\mu_{in}$. The final distribution of BH mass ratios is shown in Fig. 5 for $\Delta_m = 0.1, 0.3$, and 0.5 . In the upper

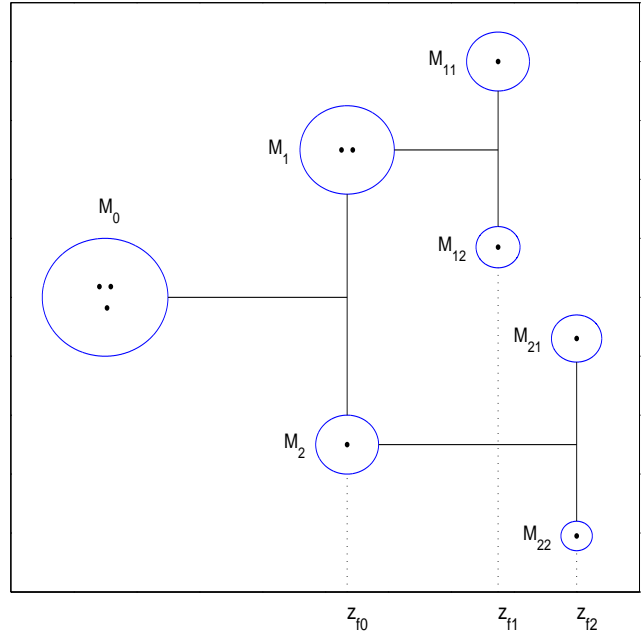


Figure 4. Schematic diagram of our algorithm for generating the BH mass distribution. First we select a formation time z_{f0} for the halo M_0 hosting the BH triple system randomly from equation (19). Given z_{f0} and $M(z_{f0})$, we select two progenitor masses M_1 and M_2 according to equation (20), assign the binary to the larger one and the third BH to the smaller one. We repeat this process going back one step further in the ‘merger tree’ to get the masses of the binary constituents.

panel we plot the inner binary mass ratios, while the lower panel shows the distribution of m_{bin}/m_{esc} , where m_{esc} is the mass of the lightest BH and m_{bin} is the sum of the masses of the other two BHs. This ratio determines the binary recoil speed when the lightest BH is ejected from the system. The total BH mass is typically $\sim 6 \times 10^8 M_\odot$ in our canonical runs.

2.2 Stellar spheroid model

To complete the galactic model we surround the BH system by a smooth stellar potential superimposed on the dark matter halo. The stars are modelled using the ‘ η -models’ of Tremaine et al. (1994), with a sharp break to shallower slope $-\gamma$ added at $r_b \ll a$:

$$\rho(r) = \begin{cases} \frac{\eta}{4\pi} \frac{Ma}{r^{3-\eta}(r+a)^{1+\eta}} \equiv \rho_\eta(r), & \text{if } r > r_b; \\ \rho_\eta(r_b)(r/r_b)^{-\gamma} & \text{if } r < r_b. \end{cases} \quad (25)$$

Our canonical model is the $\eta = 2$ (Hernquist) profile, and we also try $\eta = 1.5$ (runs SC) to explore the effect of a steeper inner profile and higher central density ($\rho \sim 800 M_\odot \text{ pc}^{-3}$ for $\eta = 1.5$ vs. $\rho \sim 180 M_\odot \text{ pc}^{-3}$ for the Hernquist profile at the BH radius of influence). r_b and γ were initialized by an estimate of the cusp destruction caused by the inspiralling BHs in reaching their initial configuration, and were updated throughout the simulation to account for the continued core heating and mass ejection. Our algorithm for updating the core is described further in §3.5.

The parameters M and a in the η -models were set

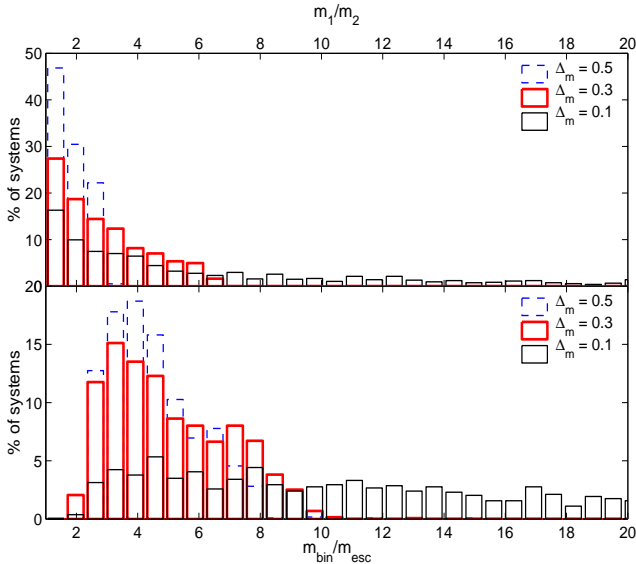


Figure 5. Distribution of BH binary mass ratios. Upper panel: Inner binary mass ratio $m_1/m_2 > 1$. Lower panel: $m_{\text{bin}}/m_{\text{esc}}$, where m_{esc} is the mass of the lightest BH and m_{bin} is the sum of the masses of the other two BHs.

based on the tight correlations observed between SMBH mass m_{bh} and stellar bulge mass (Magorrian et al. 1998; Marconi & Hunt 2003; Peng et al. 2005) and velocity dispersion (Ferrarese & Merritt 2000; Gebhardt et al. 2000; Tremaine et al. 2002). Marconi & Hunt (2003) found the relation $M_{MH03} = (4.06 \times 10^{10} M_{\odot})(m_{bh}/10^8 M_{\odot})^{1.04}$ between m_{bh} and the virial mass $M_{vir} = kR_e\sigma_e^2/G$ of the stellar bulge, where R_e is the half-light radius and σ_e is the effective bulge velocity dispersion. They set $k = 3$ (k would be $8/3$ for an isothermal sphere) to get an average ratio of unity between M_{vir} and the dynamically measured masses M_{dyn} of galaxies with more direct stellar-dynamical mass determinations (Gebhardt et al. 2003). σ_e is typically measured over either a circular aperture of radius $R_e/8$ (Ferrarese & Merritt 2000) or a linear aperture out to R_e (Gebhardt et al. 2000) – Tremaine et al. (2002) discuss the essential agreement between the velocity dispersions measured in these two ways. Thus for each model ($\eta = 2, 1.5$) we first compute the projected radius $R_e \equiv \kappa_1 a$ containing half the integrated surface brightness, and velocity dispersion $\sigma_e^2 \equiv \kappa_2 M/a$ at radius $R_e/8$. Here κ_1 and κ_2 are constants depending on the density profile (see Tremaine et al. 1994 for relevant formulae). The parameter M is then chosen to satisfy $3R_e\sigma_e^2 = 3\kappa_1\kappa_2 M = M_{MH03}(m_{bh}) \Rightarrow M = M_{MH03}/(3\kappa_1\kappa_2)$. For the Hernquist model with $\kappa_1 = 1.815$ and $\kappa_2 = 0.104$, $M_H = 1.76M_{MH03} = (7.15 \times 10^{10} M_{\odot})(m_{bh}/10^8 M_{\odot})^{1.04}$. The scale radius is then obtained from $a = M_{MH03}/3\kappa_1\sigma_{bh}^2(m_{bh})$, where $\sigma_{bh}(m_{bh})$ is the velocity dispersion computed from the $m_{bh} - \sigma$ relation of Tremaine et al. (2002). In each of these relations m_{bh} is set to the total mass of the triple BH system.

In a perfectly smooth, spherically symmetric galactic potential, BHs ejected on distant radial orbits return directly to the center to interact strongly with any other nuclear black holes. Since real galaxies are clumpy and triax-

ial, the interaction will more realistically be delayed until the orbit of the ejected BH decays by dynamical friction. To mitigate this problem we flattened the η -models by adding two low-order spherical harmonic terms to the spherical potential (de Zeeuw & Carollo 1996):

$$V(r) = u(r) - v(r)Y_2^0(\theta) + w(r)Y_2^2(\theta, \phi), \quad (26)$$

where $u(r)$ is the potential of the spherical η -model, $v(r) = -GMr_1r^{\eta-1}/(r + r_2)^{\eta+1}$, and $w(r) = -GMr_3r^{\eta-1}/(r + r_4)^{\eta+1}$. Since near-sphericity in the inner regions is probably a necessary prerequisite for the survival of the inner binary for of order a Hubble time until the next merger (Merritt & Poon 2004; Berczik et al. 2006), the parameters r_1, \dots, r_4 were chosen to give a spherical profile near the galactic center, and axis ratios approaching 1.3 and 1.5 for $r \gg a$. A similar triaxial modification was applied to the dark matter halo, and the relative orientation of the stellar and halo potentials was chosen randomly. By misaligning their axes we eliminate any artificial stable orbits (e.g. along the long axis of an ellipsoid) near which ejected BHs tend to return on a perfectly radial orbit to the center. This triaxial modification had the desired effect of preventing frequent strong encounters at pericentre on distant orbits, but had little influence on the global outcome statistics.

2.3 Initial BH configuration

We assume that the three-BH system starts off as a hierarchical triple on the verge of unstable three-body interactions. In our canonical runs we initialize the inner binary semi-major axis a_{in} to a_{hard} . To study the effect of varying a_{in} we also try runs with $a_{in} = 3r_h$ (runs BA) and $a_{in} = r_h/3$ (runs SA). The outer binary semi-major axis a_{out} is set by the stability criterion of Mardling & Aarseth (2001), equation (11). The initial eccentricity of the inner (outer) binary was chosen uniformly between 0.0 and 0.2 (0.3), in accordance with the low eccentricities found in galaxy merger simulations where dynamical friction tends to circularize the orbits of satellites as they spiral inward (Milosavljevic & Merritt 2001). The three Euler angles of the intruder's orbital plane were chosen randomly relative to the reference plane of the binary orbit, as was the phase of the initial periastron of the binary. Both orbits were always started at pericentre; since many orbital periods elapse before unstable interactions begin, the relative phase is effectively randomized in any case. Having defined an initial configuration of three BHs embedded in a stellar+dark matter potential, we next describe how we evolve the system forward in time.

2.4 Code method

We treat the three-body interactions using Sverre Aarseth's *Chain* code, which is optimized for the efficient and accurate integration of close few-body encounters. When the binary and third body are far apart we switch to unperturbed two-body motion using a 4th-order Runge-Kutta (RK4) method with variable timesteps, and simultaneously evolve the binary semi-major axis and eccentricity using orbit-averaged equations to describe the effects of gravitational radiation and energy loss to the stars. The majority of the computation time is spent on the close encounters. Until the binary

pair coalesces, the relative perturbation to the binary from the third body at apocentre,

$$\delta F = \frac{2r_{ap}^3 m_3}{\min(m_1, m_2) d^3}, \quad (27)$$

is used to decide which integration method to use at any given time. Here r_{ap} is the apocentre distance between m_1 and m_2 , m_3 is the intruder mass, and d is the distance of the intruder from the binary center-of-mass. We switch to two-body RK4 integration each time δF falls below 5×10^{-5} and call the *Chain* code again when δF reaches 5×10^{-4} . We choose different δF thresholds for beginning and ending close encounters to prevent overly frequent toggling between the two methods. When < 3 BHs remain in the simulation (after coalescence of the inner binary or escape of one or more BHs from the galaxy), we primarily use the RK4 integrator, but call the *Chain* code to treat very close two-body encounters. Since chain regularization is defined only for three or more bodies, we add a light and distant “dummy” particle when using this method for two-body motion.

The *Chain* code is an implementation of the N-body regularization technique of Mikkola and Aarseth (Mikkola & Aarseth 1990, 1993), which first orders the masses so that neighbors in the chain are the dominant two-body interactions, then applies the KS-transformation (Kustaanheimo & Stiefel 1965) to neighboring pairs. This transformation eliminates the singularity at $r \rightarrow 0$ in Newtonian gravity and transforms the equations of Keplerian motion to the simple harmonic oscillator equation (Stiefel & Scheifele 1971). External perturbing forces of arbitrary strength depending on the coordinates, velocities, and/or time are simply incorporated into the formulation (though of course singularities in these perturbing forces need not be eliminated by the change of variables). The code uses the Bulirsch-Stoer (BS) method (Bulirsch & Stoer 1966) based on Romberg extrapolation to integrate the regularized equations of motion, allowing the code to take large timesteps and save substantially on computation time. For unperturbed sinusoidal motion, the BS integrator takes only two or three timesteps per orbital period! The *Chain* code’s efficient treatment of close multi-body encounters is especially needed in our calculations since the system starts off as a hierarchical triple, leading to complex resonant encounters lasting many dynamical times in every run.

We modify the *Chain* code to include three external perturbing forces in addition to Newtonian gravity. First we add a galactic potential consisting of a stellar component plus a dark matter halo, modelled by the density profiles described in previous sections. Next we model the energy transfer to the stars as a dynamical friction force given by Chandrasekhar’s formula (Chandrasekhar 1943; Binney & Tremaine 1987),

$$\vec{F}_{df} = -\frac{4\pi \rho m \ln \Lambda [\text{erf}(X) - 2X e^{-X^2} / \sqrt{\pi}]}{v^2} \vec{v} \quad (28)$$

where $X \equiv v/(\sqrt{2}\sigma)$. The factor in square brackets ≈ 1 for $v \gg \sigma$ and $\approx 0.75X^3$ for $v \ll \sigma$. We set $\ln \Lambda = 1$. For ρ we use the density evaluated at the BH’s radius of influence, $r_{inf} = Gm/\sigma^2$. r_{inf} approximately marks the boundary between the stellar cusp that moves with the BH and the background stars exerting a drag on the bound hole+cusp complex.

We checked the results’ sensitivity to the dynamical fric-

tion prescription by trying three different implementations of equation (28): (i) applying the drag force separately to each BH during all of the close encounters; (ii) applying it only to the intruder during the first encounter until the onset of unstable interactions (defined loosely by the first time the closest pair is not formed by the original inner binary members); and (iii) employing a “hierarchical” dynamical friction prescription in which equation (28) was applied separately to the inner and outer binaries until the onset of strong interactions, defined as in (ii). All three prescriptions gave similar results, so we concluded that the details of the drag implementation during close encounters are not important. In our final runs we adopted prescription (ii), since it is the most conservative with respect to stellar hardening of the binary and core scouring by the SMBHs. All encounters after the first one typically proceed too quickly and at binding energies too high for significant stellar dissipation, so in practice prescriptions (i-iii) only differ in the way the first encounter is handled. We do not allow the outer binary to stall *before* the onset of strong interactions in our simulations, consistent with our tactic of *assuming* that such interactions occur.

Finally we incorporate gravitational radiation drag using the $\mathcal{O}[(v/c)^5]$ post-Newtonian (2.5PN) back-reaction acceleration computed by Damour & Deruelle (1981). We evaluate the acceleration in the two-body center-of-mass frame (e.g. Gultekin et al. 2006),

$$\frac{d\vec{v}_1}{dt} = \frac{4G^2}{5c^5} \frac{m_2}{m_1 + m_2} \frac{m_1 m_2}{r^3} \left\{ \hat{r}(\hat{r} \cdot \vec{v}) \left[\frac{34G(m_1 + m_2)}{3r} + 6v^2 \right] + \vec{v} \left[-\frac{6G(m_1 + m_2)}{r} - 2v^2 \right] \right\} \quad (29)$$

where $\vec{r} = \vec{r}_1 - \vec{r}_2$ and $\vec{v} = \vec{v}_1 - \vec{v}_2$ are the relative positions and velocities of the two masses. We sum the force linearly over all pairs, a valid approximation provided the perturbations from the third body and other external tidal forces are instantaneously small at pericentre. When averaged over a complete orbit, equation (29) is equivalent to the Peters (1964) equations for the binary semi-major axis and eccentricity,

$$\frac{da}{dt} = -\frac{64}{5} \frac{G^3 m_1 m_2 (m_1 + m_2)}{c^5 a^3} \frac{1 + \frac{73}{24} e^2 + \frac{37}{96} e^4}{(1 - e^2)^{7/2}} \quad (30a)$$

$$\frac{de}{dt} = -\frac{304}{15} \frac{G^3 m_1 m_2 (m_1 + m_2)}{c^5 a^4} \frac{e + \frac{121}{304} e^3}{(1 - e^2)^{5/2}}. \quad (30b)$$

However when $|\hat{v} \cdot \hat{r}|$ comes close to one on hyperbolic orbits, so that $(\hat{r} \cdot \vec{v})^2 \rightarrow v^2$, $\dot{E} = \vec{F}_1 \cdot \vec{v}_1 + \vec{F}_2 \cdot \vec{v}_2 = m_1 \vec{a}_1 \cdot \vec{v}$ as given by equation (29) becomes *positive*, though we know physically that gravitational waves can only carry energy away from the system. To give the correct answer averaged over an orbit, this positive contribution must be cancelled by extra energy loss near pericentre, making the equation potentially sensitive to numerical error. This effect is much less pronounced in the Damour & Deruelle (1981) form than in expressions for the radiation back-reaction acceleration derived by other authors - they derived the formula specifically for practical use on the problem of two point masses (see Appendix of Lee 1993 and references therein). The code tests in the next section verify the suitability of this form for our calculations.

For computational ease we neglect the lower-order 1-2PN terms (precession of the periastron) in the post-

Newtonian expansion. Though much larger in magnitude than the radiation reaction force, these terms are unimportant in the statistical sense because they conserve the intrinsic properties of the system, such as energy (Kupi et al. 2006; Iwasawa et al. 2005). We need not concern ourselves with relativistic precession destroying the Kozai resonance since the semi-major axis ratio given by equation (11) is much smaller than that of equation (9).

When δF falls below 5×10^{-5} we replace the binary pair (m_1, m_2) with a single body of mass $m_{bin} = m_1 + m_2$ and the binary center-of-mass position and velocity, and continue following the motion of m_{bin} and m_3 through the galaxy with the RK4 integrator. In addition to the two-body attraction and galactic potential, we apply a dynamical friction force given by equation (28) with

$$\ln \Lambda = \ln \left[\frac{r(\sigma^2 + v^2)}{Gm} \right] \quad (31)$$

to each of m_3 and m_{bin} , where r is the BH's distance from the galactic center. As in the close encounters, we cap the density at $\rho(r_{inf})$ when the BHs pass through the core. We evolve the binary semi-major axis and eccentricity as $da = [(da/dt)_{st} + (da/dt)_{gw}]dt$, $de = [(de/dt)_{gw}]dt$, where $(d/dt)_{st}$ and $(d/dt)_{gw}$ are the contributions from stellar interactions and gravitational radiation. $(da/dt)_{gw}$ and $(de/dt)_{gw}$ are given by equation (30), and the stellar treatment is based on the work of Quinlan (1996).

Through an extensive series of three-body scattering experiments, Quinlan (1996) deduced the hardening rate

$$\left(\frac{da}{dt} \right)_{st} = -\frac{\rho Ha^2}{\sigma} \quad (32)$$

of a massive binary in a uniform sea of stars with velocity dispersion σ , as a function of the binary orbital velocity v_{bin} and mass ratio m_1/m_2 over the range of values relevant for SMBH binaries. He identified $w = 0.85\sqrt{G \min(m_1, m_2)/a}$ as the characteristic velocity distinguishing the hard binary regime - stars with $v \gtrsim w$ cannot be easily captured into bound orbits and preferentially harden the binary in close encounters. He focused on the hard binary ($w \gg \sigma$) and transition ($w \sim \sigma$) regimes where Chandrasekhar's formula ceases to apply. The velocity dependence of the hardening rate is absorbed in the parameter

$$H \approx \frac{16}{[1 + (\sigma/w)^4]^{1/2}}. \quad (33)$$

In our simulations the binary center-of-mass is often speeding through the stellar medium at $v_{cm} \gtrsim \sigma$ after an energetic ejection, so the stellar medium looks "hotter" in its frame of reference. To account for this we replace σ in equations (32) and (33) with $\sigma^* \equiv \sqrt{v_{cm}^2 + \sigma^2}$, a good approximation since H is not very sensitive to the shape of the distribution function (e.g. $H \approx 16$ for a Maxwellian vs. $H \approx 18$ for a uniform velocity distribution). For ρ in equation (32) we took $\min[\rho(r), \rho(r_{inf})]$ as we did for the drag on the center-of-mass. We ignored the mild eccentricity evolution $(de/dt)_{st}$, which is shown in Quinlan (1996) to be far weaker than that predicted by Chandrasekhar's formula for hard eccentric binaries.

The timesteps are adaptively controlled with a simple step-doubling scheme: at each step the 14 numbers $\{x_1, \dots, x_6; v_1, \dots, v_6; a, e\}$ are all required to remain the same to within an error $\epsilon = 10^{-n}$ under doubling of the step size.

To avoid wasting computation time when any of these values approach zero, we accept agreement to n decimal places as an alternative criterion for convergence. For the calculations reported in this paper we set $n = 12$.

When one of the two masses settles to the center by dynamical friction (its amplitude falls below $Gm/2\sigma^2$), we stop integrating its motion and place it at rest at the galactic center until the second body returns to within a distance of twice the break radius, $2r_b$. If the settled mass is the binary, then we also stop updating its semi-major axis for stellar hardening, assuming that it clears out its loss cone and stalls once it stops encountering new stars by moving about the nucleus. Since the total mass in loss cone stars is small compared to the BH mass in the low-density galaxies that we consider, to good approximation the binary stalls as soon as the replenishing mechanism (motion) shuts off.

We declare the binary to have coalesced when $|a/\dot{a}|_{gr} = (5/256)\dot{a}^4 f(e)/G^3 \mu m_{bin}^2 < 200$ yrs during the RK4 integration, $|a/\dot{a}|_{gr} < 0.1 t_{dyn}$ during a close encounter, or $r_{12} < 1.1(r_{s1} + r_{s2})$ at any point, where t_{dyn} is the current outer binary dynamical time, and $r_{s1,2}$ are the Schwarzschild radii of the two binary members. Upon coalescence we replace the pair with a single body of mass m_{bin} and the center-of-mass position and velocity. We also try adding isotropic velocity kicks of magnitude $v_{kick} = 250g(\eta)/g(\eta_{max})$ km/s, where $g(x) = x^2 \sqrt{1-4x}(1.0912 - 1.04x + 2.92x^2)$ and $\eta = m_1 m_2 / (m_1 + m_2)^2$, to represent the net linear momentum kick that a coalescing binary receives due to the beaming of the radiation along the direction opposite the smaller BH's velocity (Favata et al. 2004; Merritt et al. 2004; Blanchet et al. 2005). Here $\eta_{max} \approx 0.20$ is the mass ratio giving the maximal kick. However the characteristic velocities in the massive galaxies that we consider are substantially higher than v_{kick} , and so the kicks have very little effect on the outcomes.

A run ends when one of the following termination conditions is met: (a) The single BH m_3 has escaped the galaxy ($r > 500$ kpc and $E = \Phi(r) + \frac{1}{2}v^2 > E_{esc}$) and the binary (remnant) m_{bin} has settled to the center by dynamical friction; (b) m_{bin} has escaped and m_3 has settled to the center; (c) both m_3 and m_{bin} have escaped the galaxy; (d) the original binary has coalesced and a new, hard binary has formed out of m_{bin} and m_3 ; (e) the (m_3, m_{bin}) system has coalesced and only one BH remains at the galactic center; (f) the physical run time exceeds $t_{max} = t_0 - t_{f0}$, the current age of the universe minus the halo formation time; or (g) the physical time spent in a call to *Chain* exceeds a maximum allowed time t_{chn} . The last condition is added to avoid spending too much computation time on very long close encounters.

2.5 Note on the stellar treatment

During the unperturbed binary evolution we used Chandrasekhar's formula to model the dynamical friction on the single BH and binary center-of-mass, and the orbit-averaged prescription of Quinlan (1996) to evolve the binary semi-major axis under stellar hardening. Though the details (e.g. the effect of the radial variation of the density) are uncertain by a factor of a few, this scheme captures the essence of the effect of the stars fairly well. However an orbit-averaged prescription is not feasible during the close encounters, so

we used a drag force given by equation (28) to bring in the intruder at the beginning of each run.

Chandrasekhar's formula is obtained by summing the two-body star-BH scattering events over all impact parameters $[b_{min}, b_{max}]$ in the limit of *weak* encounters, assuming that the numerous distant encounters dominate over less common large angle scattering¹. This assumption is valid so long as the dynamical time of the BH system far exceeds the typical minimum encounter time, $t_{dyn} \gg t_{enc} = b_{min}/\sigma$. In the opposite limit, $t_{dyn} \ll t_{enc}$, distant encounters affect only the system's center-of-mass and the energy loss is dominated by strong three-body encounters ending in the high-velocity ejection of the star – in this regime the hardening rate is a property of the bound system as a whole and cannot be described as a separate force acting on each BH. There is no immediate reason to expect any relation between Chandrasekhar's formula and the hard binary decay rate.

Therefore our use of equation (28) should be viewed more as a tool to efficiently start strong three-body interactions in a hierarchical triple system on the brink of stability, than as an accurate description of the BH trajectories under the cumulative influence of the stars. Modelling the energy loss as a separate, compact force acting on each BH allows us to incorporate it easily into the *Chain* code as an external perturbing acceleration. By varying our implementation of equation (28) as described previously, we have verified that our results are not very sensitive to the dynamical friction prescription. With $\ln \Lambda \sim 1$ the rate of energy loss given by Chandrasekhar's formula is close to the value given by equations (32) and (33) at a_{hard} for the same ρ .

Given the significant ambiguities in the stellar treatment, our strategy is to choose a *conservative* estimate of the stellar dissipation so that conclusions on efficient binary coalescence with the help of the stars and core scouring by the SMBH systems will be robust. During the unperturbed binary integration we stop evolving a as soon as the binary settles to the center, assuming instant emptying of the loss cone. By starting the simulation with the binary at a_{hard} in our canonical runs and letting the drag act only on the intruder in the first encounter, we neglect the scattering of stars into the loss cone by the intruder *before* the onset of strong three-body interactions. Chandrasekhar's formula also most likely underestimates the rate of energy loss to the stars for hard binaries. For supersonic ($v \gg \sigma$), circular binaries equation (28) gives $F_{df} \propto v^{-2} \propto a$, so that the torque, $\tau \approx mv\dot{a} = rF_{df} \propto a^2$, or since $v \propto a^{-1/2}$, $a^{-1/2}\dot{a} \propto a^2 \Rightarrow t_{df} = |a/\dot{a}| \propto a^{-3/2}$. On the other hand a hard binary is defined as one that hardens at a constant rate, $|dE/dt| = \text{const} \Rightarrow |a/\dot{a}| \propto a^{-1}$. Hence if the Chandrasekhar and hard binary decay rates are about the same at a_{hard} , then the rate given by equation (28) should be *smaller* than the full loss cone hardening rate by about a factor of $\sqrt{a/a_{hard}}$.

The encounters in our runs occur primarily in the transition between the dynamical friction and hard binary

¹ This assertion is often justified by the fact that the sum over the weak encounters yields *equal contributions to the drag from equal logarithmic intervals in b* (expressed by the form $\ln(b_{max}/b_{min})$ of the Coulomb logarithm). Assuming $[b_{min}, b_{max}]$ spans many logarithmic intervals, the first one corresponding to close encounters may be neglected (e.g. Spitzer 1987).

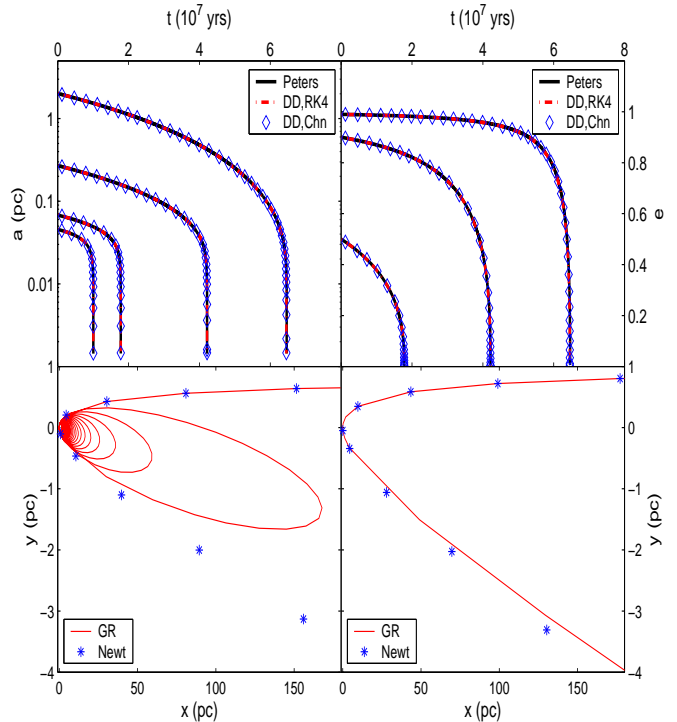


Figure 6. Code tests on the Newtonian two-body problem with gravitational radiation. Upper panels: Evolution of elliptical orbits computed using RK4 integration of the Peters equations (black solid), RK4 integration with the Damour & Deruelle (DD) radiation back-reaction acceleration (red dashed), and *Chain* integration with the DD acceleration (diamonds). The initial conditions were chosen to give $|a/\dot{a}| = 10^7$ yrs at the beginning of each integration. Left: Semi-major axis evolution for initial eccentricities of $e_0 = 0.0, 0.5, 0.9$, and 0.99 (bottom to top). Right: Eccentricity evolution for $e_0 = 0.5, 0.9$, and 0.99 . The curves' indistinguishability demonstrates the reliability of all three methods. Lower panels: Hyperbolic orbits with impact parameters b set to 80% and 120% of the critical value for gravitational radiation capture, computed using the DD acceleration in the *Chain* code. Left: $0.8b_{crit}$; BH is captured. Right: $1.2b_{crit}$; BH is not captured. The blue asterisks are points along the Newtonian trajectory (without gravitational radiation). The deviation from the Newtonian trajectory after pericentre can be seen in both plots, even though the energy remains positive in the latter.

regimes. This transition is not well understood, and is an interesting topic for future study, as it may have significant bearing on the evolution of SMBH binaries.

2.6 Code tests and energy errors

One way to establish the reliability of our integration methods is to test them on problems with known solutions. Fig. 6 shows an example on the two-body problem with gravitational radiation. The upper panels show the evolution of the semi-major axis a and eccentricity e of four decaying elliptical orbits, computed using (a) our RK4 integrator and equation (29), with an error tolerance of $\epsilon = 10^{-9}$, (b) the *Chain* code and equation (29), with $\epsilon = 10^{-14}$, and (c) the Peters (1964) equations, (30). In each case the initial semi-major axis a_0 was chosen to give a gravitational radiation timescale of $|a/\dot{a}| \approx 10^7$ yrs, and the four curves (from bot-

tom to top) are for eccentricities of 0.0, 0.5, 0.9, and 0.99. The agreement of the three computation methods demonstrates the reliability of both the RK4 integrator and our implementation of the *Chain* code in handling dissipative forces.

The lower panels show two hyperbolic orbits with pericenter distances around 30 times the Schwarzschild radius r_s of the larger BH, computed using equation (29) in *Chain*. The RK4 integrator was found to fail some tests on very close approaches from hyperbolic orbits with gravitational radiation, so we treat all such approaches using the regularized *Chain* code in our runs, even during the unperturbed binary evolution. The blue asterisks are points along the Newtonian orbits while the red solid lines show the trajectories with gravitational radiation. There is a simple analytic expression for the maximum pericenter distance for gravitational radiation capture from a hyperbolic orbit,

$$r_{p,max} = \left[\frac{85\sqrt{2}\pi G^{7/2} m_1 m_2 (m_1 + m_2)^{3/2}}{12c^5 v_\infty^2} \right]^{2/7}, \quad (34)$$

where m_1 and m_2 are the masses of the two bodies and v_∞ is their relative velocity at infinity. The orbit on the lower left begins at 80% of the critical impact parameter and the incoming BH is captured. On the right the intruding BH starts at 120% of the critical impact parameter and is not captured, though the deviation from the Newtonian trajectory due to the energy radiated at pericenter can be seen on the way out. We tried iterating over impact parameters close to the critical value and found that the code reproduces equation (34) to within a part in 10^6 for pericenter distances $r_{peri} \sim 30r_s$, and to within a part in 10^3 for $r_{peri} \sim 3r_s$.

We also evaluated the performance of the code by repeating our canonical ($\Delta_m = 0.3$, $\eta = 2$, $a_0 = a_{hard}$) set of 1005 runs with a static inner profile to check the precision of energy conservation. In Fig. 7 we histogram the energy errors, computed as

$$\epsilon = \left| \frac{E_0 + \sum_i \left[\int_{t_0}^{t_f} (\vec{F}_{df,i} \cdot \vec{v}_i + \vec{F}_{gw,i} \cdot \vec{v}_i) dt \right] - E_f}{E_0 - E_f} \right|, \quad (35)$$

where E_0 and E_f are the initial and final energies, and the two terms in the sum under the integral are the work done by dynamical friction and gravitational radiation during the current stage of the code. In the upper panel we separately plot the errors for close three-body encounters, RK4 integration of the unperturbed binary motion (“far”), and close two-body encounters computed with *Chain* during the unperturbed binary evolution. The plot includes all code stages where the energy dissipated was at least 10^{-3} in code units, or about a part in 10^{5-6} of the initial binding energy of the system. The black (heavy) histogram shows the errors for close encounters normalized to the *initial* energy instead of the dissipated energy in the denominator of equation (35), since the energy dissipated was very small in many close encounters. In the lower panel we combine the energy errors from the various code stages to get an effective energy error for each entire run,

$$\epsilon_{run} = \frac{\sqrt{\epsilon_1^2 \Delta E_1^2 + \epsilon_2^2 \Delta E_2^2 + \dots + \epsilon_n^2 \Delta E_n^2}}{\Delta E_1 + \Delta E_2 + \dots + \Delta E_n}. \quad (36)$$

We had to combine the separate errors to obtain ϵ_{run} since the galactic potential is handled slightly differently during different stages of the code, e.g. the triaxial modification is

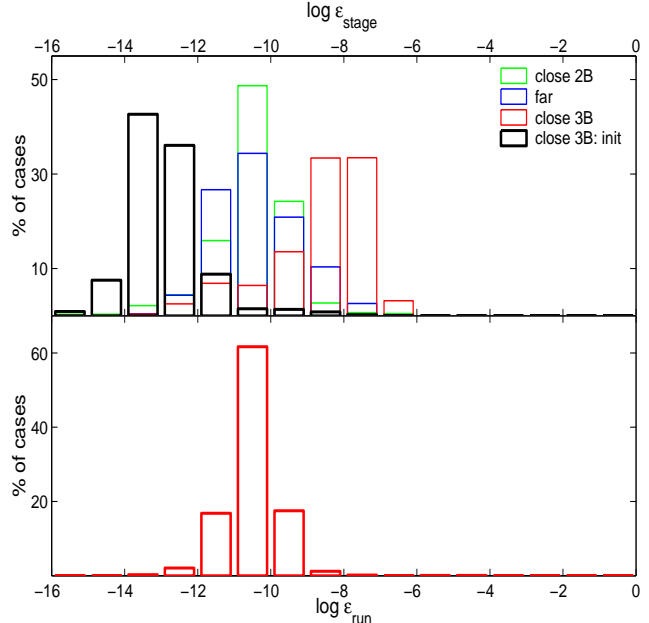


Figure 7. Energy errors. Upper panel: Errors given by equation (35), for each code stage: close triple encounters, integrated with *Chain* (red); unperturbed binary evolution with the RK4 integrator (blue); and very close two-body encounters computed with *Chain* after the binary has coalesced (green). The black (heavy) histogram shows the energy errors for close triple encounters normalized to the *initial* energy instead of the energy dissipated. Lower panel: Effective energy errors for the entire run, computed from equation (36).

applied only during the RK4 integration. In a large majority of cases ϵ_{run} falls between 10^{-12} and 10^{-9} , and energy is conserved to better than a part in 10^4 in every run. The excellent energy conservation gives us confidence in the robustness of our integration methods.

3 RESULTS

3.1 Outcome statistics

We begin with an overview of the outcomes of our three-body simulations. In subsequent sections we focus on various effects in more detail. Our data consists of eight sets of 1005 runs, each sampling a different distribution of the initial conditions (ICs). A set of 1005 runs took anywhere from ~ 4 to ~ 30 hours to finish on five 2.0 GHz Opteron processors, depending on the ICs (e.g. set SA took the longest while sets BA and SC ran very quickly, since the dissipation time is longer compared to the dynamical time for smaller a_{in} , and shorter with the higher central density in the $\eta = 1.5$ cusp).

In our canonical runs (CN), we chose $\Delta_m = 0.3$ for the threshold merger mass ratio, modelled the stellar bulge as a Hernquist ($\eta = 2$) profile, started off the inner binary at a_{hard} , and generated the ICs from a $5 \times 10^{13} M_\odot$ halo at $z = 0$. In each of the remaining runs we varied one of these assumptions. Runs D1 and D5 used $\Delta_m = 0.1$ and $\Delta_m = 0.5$ to explore the effects of widening or narrowing the range of BH mass ratios. In runs MX we assigned a mass

Table 1. Summary of outcomes for eight different distributions of the initial conditions. See text for explanation of the entries.

Outcome	CN	D1	D5	MX	BA	SA	SC	H1
Coalescence								
One pair	87%	68%	89%	84%	84%	95%	84%	75%
Two pairs	15%	13%	18%	16%	22%	13%	16%	10%
Escape								
Single	15%	18%	17%	19%	21%	14%	14%	22%
Double	0.0%	0.0%	0.1%	0.0%	0.1%	0.2%	0.1%	0.3%
Wander	37%	51%	38%	42%	42%	26%	45%	50%
Final state								
Binary	60%	67%	54%	57%	51%	65%	56%	63%
Single	38%	31%	45%	41%	47%	33%	43%	35%
No BH	1.3%	2.0%	1.2%	1.5%	1.4%	1.4%	1.2%	1.8%
Core								
$\langle M_{def} \rangle$	1.41	1.20	1.50	1.38	1.31	1.96	1.42	1.61
ΔM_{def}	0.48	0.37	0.57	0.44	0.52	0.44	0.57	0.61
Termination								
Sing escape	14%	16%	16%	18%	18%	14%	12%	21%
New binary	61%	44%	61%	55%	53%	73%	54%	49%
T.O. far	22%	30%	22%	23%	20%	12%	31%	28%
T.O. <i>Chain</i>	2.1%	10%	1.7%	4.4%	8.4%	0.3%	1.6%	1.5%
Crashed	0.5%	0.1%	0.3%	0.3%	0.7%	0.2%	0.6%	0.1%

$m_{bh}[\max(M_{21}, M_{22}), z_{f2}]$ instead of $m_{bh}(M_{21} + M_{22}, z_{f2})$ to the intruding BH, as discussed in §2.1. In runs BA and SA we started off the inner binary at $3a_{hard}$ and $a_{hard}/3$ instead of at a_{hard} . We initialized the stellar bulge to an $\eta = 1.5$ profile in runs SC, to explore the effect of a steeper inner cusp. Finally in runs H1 we generated the ICs from a 1×10^{13} M_\odot halo at $z = 0$, for total BH masses of $\sim 5 \times 10^7 M_\odot$, about an order of magnitude lower than in our canonical runs. Table 1 summarizes the outcomes.

The first two rows give the percentage of cases in which (i) one BH pair coalesced by the end of the run (i.e. by the time since the last major merger), and (ii) the remaining two BHs also coalesced within the run time. At least one pair coalesced in a large majority of the runs for each set of ICs that we tried. The new system formed from the third BH and binary remnant also coalesced in $\sim 10\text{-}20\%$ of the cases. Since we assume that stellar hardening of the new binary shuts off at a_{hard} , it can only coalesce by gravitational radiation from a highly eccentric orbit; we will discuss this topic further in §3.2 and §3.4. The coalescence rate is somewhat lower ($\sim 68\%$) in set D1, since (a) the hardening effect of the third body is lessened for more extreme mass ratios, and (b) mergers with mass ratios as low as $\Delta_m = 0.1$ are more frequent, so the run time is typically shorter. Naturally the coalescence rate is somewhat higher (95%) in runs SA, where we begin with a tighter binary ($a_0 = a_{hard}/3$, $\tau_{gw} \sim 10^{11\text{-}12}$ yrs). Coalescence is also significantly less common in runs H1. This can be understood in light of equation (3) in §1.1. The separation between the scale set by the stellar kinematics (a_{hard}) and that set by gravitational radiation (a_{gw}) is proportional to $m_{bin}^{-1/4}$. Hence in lower mass systems, coalescence is less likely relative to escape. This observation mo-

tivates future study of triple BH dynamics in much lighter systems.

The next three rows of the table give the fraction of runs in which (i) the single BH escaped the stellar bulge + halo potential, (ii) all BHs (both the single and the binary) escaped the halo, and (iii) the single BH either escaped or remained wandering far out in the halo at the end of the run. The single escaped in $\sim 15\text{-}20\%$ of the runs in all cases. If we also count runs where it remained wandering through the halo for of order a Hubble time, this fraction increases to $\sim 40\%$. Double escapes (of both the binary and the single BH) were very rare. We get more wandering BHs in set D1, since a larger fraction of the released energy is apportioned to the escaper when it is relatively lighter, the dynamical friction time is longer, and the run time is shorter. Runs SA produced less wandering BHs since the binary pair more often coalesced before the intruder had a chance to harvest much of its energy. Wandering was also more common in set H1, due to the $m_{bh}^{-1/4}$ scaling discussed in the previous paragraph. The escape fraction of course depends on the depth of the galactic potential well. Given the uncertainty and scatter in the $m_{bh} - M_{halo}$ relation and specificity of the prescription adopted, we must expect these numbers to vary somewhat in studies with different halo or stellar density models.

The entries under “final state” tell whether, at $z = 0$, the galactic center hosts (i) a stalled BH binary, (ii) a single BH, or (iii) no BHs (neither the single nor the binary has yet returned to the center by dynamical friction). About 50-70% of the runs ended with a binary at the galactic center whose gravitational radiation time exceeded the time until $z = 0$. This includes cases where (a) the single was ejected to large distance and the binary settled to the center before it hardened enough to coalesce by gravitational radiation, (b) when the inner binary coalesced during a close encounter the outer binary coalescence time exceeded the remaining run time, or (c) the single and binary remnant both returned to the center after an ejection and formed a bound pair with a long gravitational radiation time. In most of the remaining cases (30-50%) the run ended with a single BH at the galactic center, or a binary bound to coalesce before t_0 . This occurred when (a) the single was ejected to large distance and the binary (or remnant) settled to the center after having hardened to the point of coalescence through some combination of repeated interactions with the third BH and stellar dissipation, or (b) a new binary with a short gravitational radiation time formed following return from an ejection or coalescence during a close encounter. In only a small fraction (1-2%) of cases the run ended with the center empty of BHs. Note also that this happened most often in runs where the last merger occurred recently, so the total time spent with the center empty of BHs is smaller still.

The next two entries give the mean and standard deviation of the core “mass deficit” scoured out by the triple system, in units of the total BH mass m_{bh} . For a galaxy modelled as an η -model with stellar mass parameter M_s , bulge scale radius a_s and a break to inner slope γ at r_b , we

define the mass deficit M_{def} by

$$M_{def} = 4\pi \left[\int_0^{r_b} \rho_\eta(r) r^2 dr - \int_0^{r_b} \rho(r) r^2 dr \right] = M_s \left[\left(\frac{r}{r+a_s} \right)^{\eta_s} - \left(\frac{r_b}{r_b+a_s} \right)^{\eta_s} \right] - \frac{4\pi \rho_{bs} r_b^3}{3-\gamma} + \text{D.M.}, \quad (37)$$

where ρ_{bs} is the stellar density at r_b and D.M. denotes the corresponding dark matter terms. The mass deficits are highly scattered within each set of runs, with typical $M_{def}/m_{bh} \approx 1.4 \pm 0.5$. More extreme mass ratios (runs D1) tended to produce smaller cores, while a narrower mass range (runs D5) gave somewhat larger ones. The fraction of runs ending with very high mass deficits varied strongly with Δ_m ; for instance 17% of cases ended with $M_{def}/m_{bh} > 2$ for $\Delta_m = 0.5$, vs. only (11%, 4.4%) for $\Delta_m = (0.3, 0.1)$. The large cores in set SA arose mostly from enhanced core scouring during the creation of the initial hard binary, and so are more a consequence of the ICs than of the triple interactions themselves. This sensitivity of M_{def} to the binary stalling radius is an interesting point in its own right. The larger cores in runs H1 probably arise from the higher mean number of ejections and smaller fraction of runs ending in immediate coalescence as the BH mass is decreased. 21% of the runs in this set ended with $M_{def}/m_{bh} > 2$ and 8.7% ended with $M_{def}/m_{bh} > 2.5$. The subject of core scouring will be discussed in further detail in §3.5.

Both the core scouring effect and the coalescence rate induced by the encounters are significantly reduced for the extreme mass ratios in set D1. One must keep in mind, however, that halo mergers with these mass ratios are much more frequent than those above $\Delta_m = 0.3$ (see Fig. 3), so the *cumulative* effect of these events may be as high or higher than that of encounters with near-equal masses. To quantify this statement our simulations would need to be embedded in a merger tree that follows the formation of triple systems.

Finally, the last five lines in Table 1 give the statistics of the condition which formally terminated the run: (i) the single escaped the halo and the binary (or remnant) settled to rest at the galaxy center; (ii) the escaper and binary remnant formed a stalled binary or coalesced (in a few percent of these cases a bound binary never actually formed; the pair coalesced suddenly upon a very close pericenter passage from an unbound orbit); (iii) the maximum physical time $t_{max} = t_0 - t_{f0}$ was reached (in these cases one or more BH was left wandering through the halo at the end of the run); (iv) the maximum time for a close encounter ($t_{chn} = 3 \times 10^7$ yrs for our canonical runs) was exceeded; or (v) the timestep went to zero or a limit on the number of timesteps was reached at some stage of the integration, which always occurred in <1% of cases. Runs terminating on condition (iv) or (v) were left out when computing the upper entries in the table.

In this slew of runs we have varied only a few of the relevant parameters; one might also try, for instance, varying or adding scatter to the halo mass prescription, further steepening the stellar bulge profiles or adding a disk component, and exploring vastly different BH mass scales, in particular the much lower ($\sim 10^{4-5} M_\odot$) masses that may be relevant at high redshift. One of the advantages of our method is the relative ease of varying the model and ICs. This paper should be viewed as a work in progress, in which we have developed a method that can be applied to three-

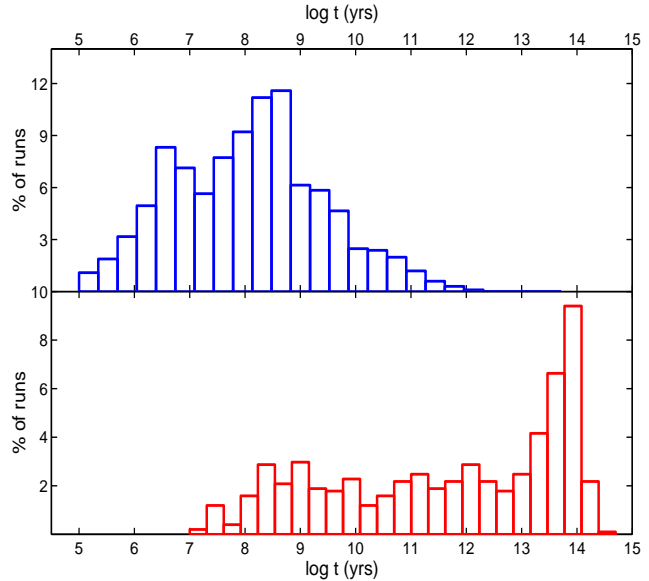


Figure 8. Distribution of coalescence times for the inner binary (upper panel) and new binary (lower panel), formed by the third body and coalesced binary remnant. The lower plot includes only runs where a new binary formed, and not e.g. cases where the single escaped or was left wandering far from the galactic center at the end of the run.

BH systems in whatever context they may arise. Given the qualitative similarity of the outcomes in the runs we've performed so far, we will focus on the canonical (CN) runs in the more detailed presentation of our results.

3.2 Efficient binary coalescence

The inner binary begins at a_{hard} , where the gravitational radiation time is $\tau_{gw} \sim 10^{13-15}$ yrs, in our canonical runs. It must shrink by a factor of ~ 10 before gravitational radiation can cause coalescence in a Hubble time, or by a factor of ~ 40 for τ_{gw} to become comparable to the dynamical friction time. The intruder helps to bridge this gap in several ways: (a) direct hardening of the binary through repeated three-body interactions, (b) enhanced stellar hardening by scattering of stars into the loss cone and motion of the binary about the nucleus, and (c) enhanced gravitational radiation losses due to thermalization of the eccentricity during the chaotic encounters and eccentricity growth via the Kozai resonance.

We find that the combination of these mechanisms leads to coalescence of the inner binary within the time $t_0 - t_{f0}$ between the merger that formed the triple system and $z = 0$ in a large majority of the runs. Our treatment of mechanism (b) is the most uncertain, so as described in §2.5 we use a conservative prescription for the stellar hardening to place an approximate lower limit on the coalescence rate. Fig. 8 shows the distribution of binary coalescence times.

The upper panel is for the inner binary, while the lower panel is for the new system formed by the third BH and binary remnant. In cases where coalescence occurred during the run, we plot the coalescence time recorded by the code. In other cases we plot $t_{run} + t_{gr,end}$, where t_{run} is the total run time and $t_{gr,end}$ is the time obtained by integrating the

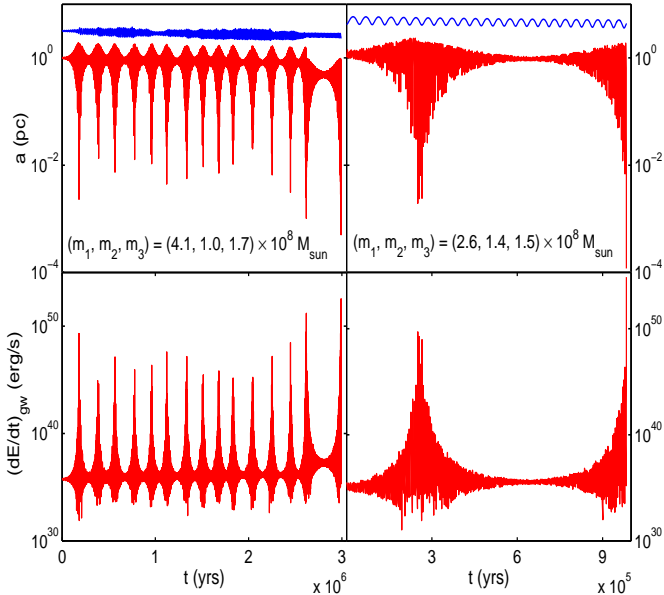


Figure 9. Two examples of rapid coalescence by Kozai oscillations. Upper panels: Time evolution of the inner (red, lower) and outer (blue, higher) binary separations. Lower panels: Total gravitational radiation power, averaged over Bulirsch-Stoer timesteps. m_1 and m_2 are the masses of the binary members and m_3 is the mass of the intruder.

Peters (1964) equations from the state at the end of the run to coalescence. The lower plot includes only those runs where the third BH ended up bound to the binary remnant, excluding, for instance, cases where the single escaped the galaxy. In $\sim 15\%$ of the runs the new binary also coalesced within the time $t_0 - t_{f0}$. Under whatever circumstances the gap-crossing mechanisms discussed in §1.1 fail, the efficient coalescence in massive triple systems provides a “last resort” solution to the final parsec problem.

3.3 The three-body interactions

Though the close encounters take up only a small fraction of the physical time in our runs, it is the energy exchanges during these encounters that determine the large-scale BH dynamics. We now take a closer look at the three-body dynamics in a few representative cases.

In $\sim 20\%$ of the runs the binary swiftly coalesces during the first encounter, usually with the help of the Kozai resonance. Two examples of this are shown in Fig. 9. The time evolution of the inner and outer binary separations is plotted for two different runs in the upper panels. For a circular orbit the separation would be roughly constant over an orbital period, or just a horizontal line in the figure. On the left the inner binary undergoes many Kozai oscillation cycles before coalescing. Observe that at the second-to-last eccentricity maximum, though it does not coalesce, the binary radiates away a large amount of energy and passes through the next eccentricity minimum with a significantly reduced semi-major axis. In the example on the right, the binary coalesces after just one full Kozai cycle. The lower panels show the time evolution of the total gravitational radiation power, averaged over the Bulirsch-Stoer timesteps. Since the system starts on the verge of chaotic interactions where the outer

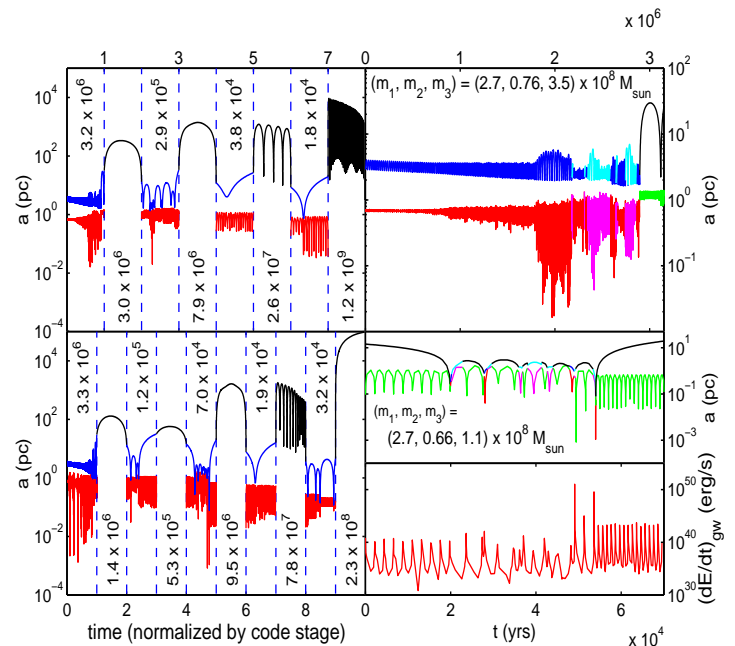


Figure 10. Two examples of longer runs. Left panels: Entire run, with time spent in each code stage normalized to unity. Actual times in years are indicated by the numbers on the plot. The red (inner binary) and blue (outer binary) portions show the close encounters, while the black portions show the calls to the RK4 integrator. Upper right: Zoom in on the first close encounter in the run at left. Lines are color-coded according to which pair is closest, to highlight the exchanges. Lower right: Zoom in on the third close encounter of the lower run, showing also the total gravitational radiation power averaged over Bulirsch-Stoer timesteps. See text for further explanation of this figure.

to inner binary semi-major axis ratio is small (so that the quadrupolar approximation breaks down), we get “messy” Kozai oscillations which can give way to catastrophic eccentricity growth at an unpredictable time.

Fig. 10 shows two examples of more complex runs. The left panels summarize the entire run, including all of the close encounters and ejections in between. Each call to the *Chain* code or the unperturbed binary integrator is separated by dashed vertical lines. The total time in each stage is normalized to unity in order to see the full history of the run at once, and not just distant ejections. The numbers on the plot are the actual times (in yrs) spent in each stage.

Each run begins with a short period of secular evolution (illustrating the remarkable stability of hierarchical triples even slightly within the Mardling-Aarseth boundary). Dynamical friction brings the intruder in a bit further to get chaotic interactions underway. This can be seen more clearly in the upper right panel, where we zoom in on the first close encounter at left. In this panel we also color-code the lines according to which two BH instantaneously form the closest pair, to show the numerous exchanges that occur during close encounters. Large-amplitude Kozai oscillations are present in the first encounter of the lower run, but no oscillations are seen in the upper run, where the initial inclination is below the critical angle.

After the first encounter, in both runs the outer components suffer a few “near” (~ 0.1 -1 kpc) ejections before

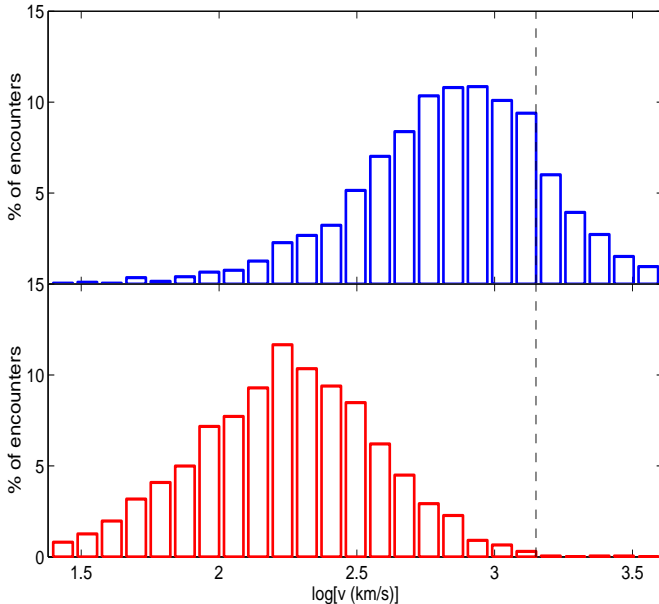


Figure 11. Distribution of ejection velocities. Upper panel: Single BH. Lower-panel: Binary center-of-mass. The total BH mass is typically $\sim 6 \times 10^8 M_\odot$.

they get shot out to kpc scales and come back by dynamical friction. In the upper run, the single goes out to ~ 10 kpc, then comes back and forms a bound pair with the former binary, which has coalesced in the meantime. The new binary is highly eccentric ($e \sim 0.9998$) and quickly coalesces by gravitational radiation. In the lower run the single returns after the first kpc-scale ejection, strongly interacts with the binary one more time, and then escapes the galaxy. The binary has a semi-major axis of 0.15 pc at the beginning of the final encounter, and its binding energy increases by 17% in the interaction, imparting a velocity of ~ 1400 km/s to the escaper.

In the lower right two panels we focus on the third encounter of this run, which was selected because a significant amount of energy was lost to gravitational radiation over its duration. We can see that the radiation loss occurred during two very close approaches, by two different BH pairs. If close three-body encounters between BHs are sufficiently common in the universe, such gravitational radiation spikes could be detectable with LISA. Note that the first encounter ($t \sim 10^{6-7}$ yrs) generally takes much longer than the later encounters ($t \sim 10^{4-5}$ yrs).

Fig. 11 shows the distribution of post-encounter velocities, for the single and recoiling binary. The ejection speed of the escaper is calculated as

$$v_{ej} = \sqrt{\frac{1}{2} |\vec{v}_s - \vec{v}_{cm}|^2 - \frac{2Gm_s}{\left(1 + \frac{m_s}{m_{bin}}\right) |\vec{r}_s - \vec{r}_{cm}|}}, \quad (38)$$

where m_s , \vec{r}_s , and \vec{v}_s , are the mass, position, and velocity of the single BH at the end of the encounter, m_{bin} is the mass of the binary, and \vec{r}_{cm} and \vec{v}_{cm} are the center-of-mass position and velocity of the three-body system. The binary recoil speed is computed analogously. This is a slight underestimate, since the galactic potential slows the BHs down a bit by the end of the encounter. Included in the plot are

all close encounters in which (a) the binary and single are unbound at the end of the encounter; (b) the binding energy of the binary increases by at least 5% (to avoid numerous “glancing” encounters where δF just barely exceeds the close encounter threshold), and (c) the encounter ends by δF falling below threshold (and not e.g. by coalescence of the binary or timing out). The dashed vertical line indicates the typical galactic (stellar bulge + halo) escape velocity, $v_{esc} \sim 1400$ km/s. We see that the single will sometimes escape the galaxy (or be ejected far out into the halo where the dynamical friction return time exceeds a Hubble time), but the binary will rarely go far.

Another point of interest is the statistics of the closest approach distances between two-body pairs during the encounters. Besides their intrinsic significance, the distances of closest approach are related to the extent of tidal stripping of the BHs during the encounters. One can imagine that if some stars, or even the inner portion of an accretion disk, remained bound to the individual BHs at the end of an encounter, then some ejected SMBHs might become observable.

Since Bulirsch-Stoer timesteps are not at all infinitesimal (see §2.4), we cannot simply take the minimum over the discrete timesteps to be the closest approach distance. When the relative perturbation δF from the third body is small, we can obtain the pericentre distance analytically in the Keplerian two-body approximation. When δF is larger, the minimum over the timesteps should give a better estimate since the timesteps tend to be smaller, but this statement is difficult to quantify. To construct the distance of closest approach in our simulations, we first identify any step where $d|r|/dt = \hat{r} \cdot \vec{v}$ switches sign from negative to positive and $|r| < 30000(r_{s1} + r_{s2})$ for any pair as a “passing step” containing a close approach. Here $\vec{r} = \vec{r}_1 - \vec{r}_2$, $\vec{v} = \vec{v}_1 - \vec{v}_2$, and $r_{s1,2}$ are the Schwarzschild radii of the two pair members. We then iteratively bisect the timestep, evaluating $\hat{r} \cdot \vec{v}$ at each bisection to find the place where it switches sign until the distance between the two bodies converges to within a part in 10^6 .

Fig. 12 shows the distribution of closest approach distances, for the closest and second closest pair, in units of (a) the initial binary semi-major axis and (b) the sum of the Schwarzschild radii of the two pair members. The plot includes the same set of encounters as Fig. 11. Since the histogram excludes encounters ending in coalescence, the lower end is truncated by gravitational radiation, while the upper end is quenched by the constraint that the binding energy increase by at least 5%.

In Fig. 13 we cast the close encounter statistics in terms of the tidal stripping question posed above. The plot shows the distribution of the tidal radius r_{tid} at closest approach, defined by the equation

$$\delta a_{tid} \equiv \frac{Gm_2}{(d - r_{tid})^2} - \frac{Gm_2}{d^2} = \frac{Gm_1}{r_{tid}^2}, \quad (39)$$

where m_1 is the reference mass being stripped (the smaller pair member), m_2 is the other point mass, and d is the distance between m_1 and m_2 . We solve this polynomial equation for r_{tid} exactly rather than Taylor expanding about $r_{tid}/d = 0$ to get the familiar expression $r = (m_1/2m_2)^{1/3}$ for the tidal radius, since r_{tid}/d is not generally small at closest approach for the near-equal mass problem at hand.

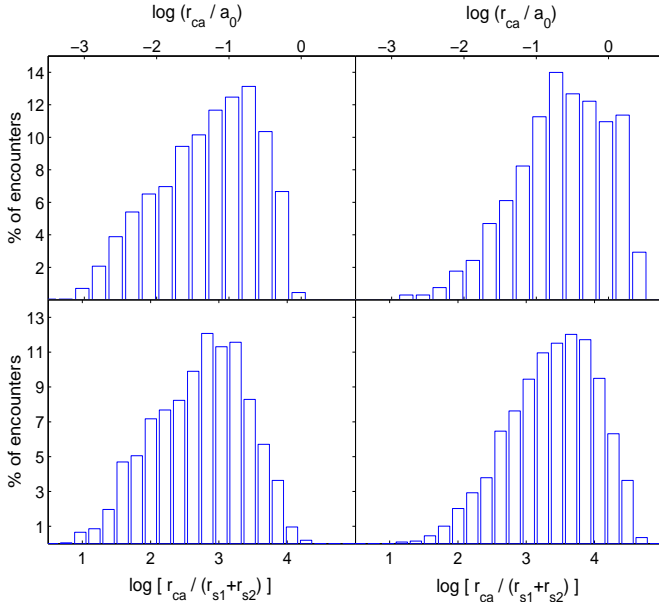


Figure 12. Distances of closest approach between pairs during close triple encounters. Upper panels: Closest approach in units of the initial inner binary semi-major axis. Lower panels: Closest approach in units of the sum of the Schwarzschild radii of the pair members. Left panels: Closest pair. Right panels: 2nd closest pair. Included are all close encounters in which the binding energy of the binary increased by at least 5%, the encounter ended by the $\delta F > 5 \times 10^{-5}$ criterion (and not by coalescence of the binary or timing out), and the third BH was not bound to the binary at the end of the encounter.

Since we are interested in observing ejected SMBHs, we only include encounters where the single escaped with a velocity above 940 km/s, the typical velocity needed to reach the stellar scale radius of ~ 3 kpc in our galactic model, in this plot. The upper panels show r_{tid} in units of the Schwarzschild radius of the smaller BH. The red circles indicate the percent of this BH's mass contained within r_{tid} in an α -disk accreting at the Eddington rate \dot{m}_{Edd} , assuming $\alpha = 0.1$ and a radiative efficiency of $\epsilon = 0.1$. The lower panels give r_{tid} in pc, and here the red circles show the mass in stars (in M_\odot) contained within r_{tid} in the Hernquist profile used to model the stellar component of the galaxy. Left panels: Closest pair; Right panels: 2nd closest pair. Included encounters are as in Fig. 12.

The enclosed masses in the upper panel were computed using the standard thin-disk accretion model (Shakura & Sunyaev 1973; Frank, King, & Raine 2002; Narayan 2003). To permit analytic solution of the fluid equations the disk is divided into three zones in which different terms may be neglected: (i) the “outer disk,” where gas pressure dominates over radiation pressure and the opacity is dominated by free-free absorption; (ii) the “middle disk” in which gas pressure is still dominant but the opacity is due primarily to electron scattering; and (iii) the “inner disk” where radiation dominates the pressure and electron scattering sets the opacity. The solution for the surface density in each of the three zones is

$$\Sigma_{out}(r) = 2.2 \times 10^9 \alpha^{-4/5} \dot{m}^{7/10} m^{1/5} r^{-3/4} M_\odot \text{ pc}^{-2} \quad (40a)$$

$$\Sigma_{mid}(r) = 4.6 \times 10^8 \alpha^{-4/5} \dot{m}^{3/5} m^{1/5} r^{-3/5} M_\odot \text{ pc}^{-2} \quad (40b)$$

$$\Sigma_{in}(r) = 2.0 \times 10^3 \alpha^{-1} \dot{m}^{-1} r^{3/2} M_\odot \text{ pc}^{-2} \quad (40c)$$

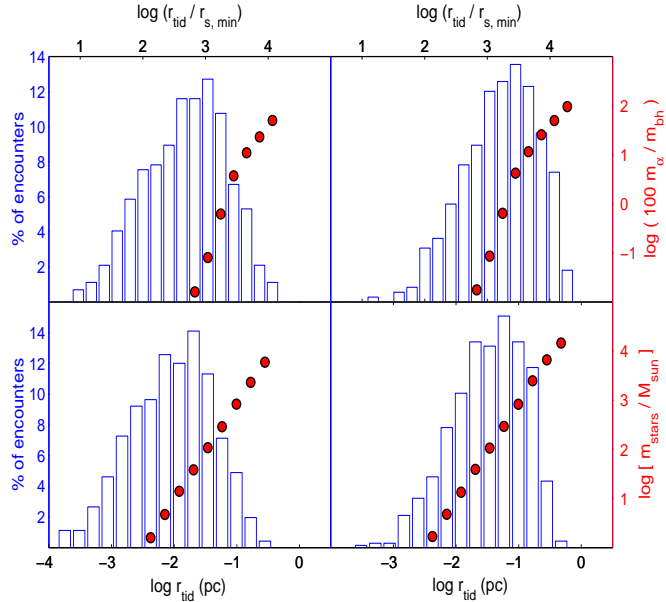


Figure 13. Tidal radius r_{tid} of the lighter pair member at closest approach. In this plot we include only encounters where one BH escaped at a speed above 940 km/s. Upper panels: r_{tid} in units of the Schwarzschild radius of the lighter pair member, $r_{s,min}$. For reference, the red circles show the percent of the BH's mass contained within r_{tid} in an α -disk if the BH is accreting at the Eddington rate \dot{m}_{Edd} , averaged over the encounters in each bin. Lower panel: r_{tid} in pc. Red circles show the mass in stars (in M_\odot) contained within r_{tid} in the Hernquist profile used to model the stellar component of the galaxy. Left panels: Closest pair; Right panels: 2nd closest pair. Included encounters are as in Fig. 12.

where m is the BH mass in M_\odot , \dot{m} is the accretion rate in units of \dot{m}_{Edd} , r is the distance from the BH in Schwarzschild radii, and α is the standard thin-disk viscosity parameter which we set to $\alpha = 0.1$. The boundary between the middle and inner zone is given approximately by $r_{mi} = 3.6 \times 10^2 \alpha^{2/21} \dot{m}^{16/21} m^{2/21}$, and the boundary separating the outer from the middle disk is around $r_{om} = 2.6 \times 10^4 \dot{m}^{2/3}$. We have left out the factor $f_* \equiv (1 - \sqrt{r_*/r})^{1/4}$, where r_* is the surface radius of the accreting object, since for a BH f_* is always small. The mass contained within radius r in the accretion disk is then $M_\alpha(r) = \int_{3r_*}^r 2\pi r \Sigma(r) dr$ where we take the innermost stable circular orbit for a non-spinning BH, $3r_*$, for the inner edge of the accretion disk.

The α -disk model assumes that the disk is not self-gravitating and breaks down as $\dot{m} \rightarrow \dot{m}_{Edd}$, so the red circles in the upper panels are merely to give the reader an idea of the bound mass scales associated with the approaches. The tidal approximation is a pessimistic estimate of the extent of the stripping since swift, one-time close passages would be impulsive. We record only the single closest approach, so we cannot distinguish between such impulsive events and approaches that are part of periodic patterns in our data.

In a significant fraction of cases $r_{tid} \gtrsim 10^4 r_s$ encloses a substantial fraction of the BH's mass in accreting gas, so near-Eddington accretion could continue for a duration of order the Salpeter (1964) time after the slingshot ejection (Hoffman & Loeb 2006). The enclosed stellar mass shown in the lower panels is never nearly comparable to the BH mass,

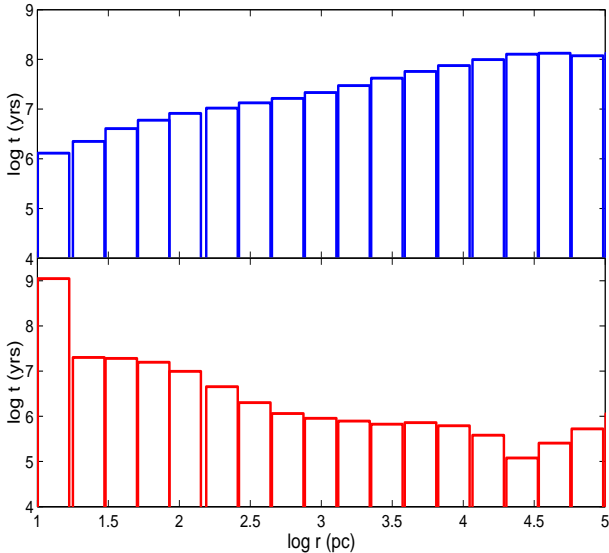


Figure 14. Total time spent by the single BH (upper panel) and binary (lower panel) at various distances from the galactic center during the run time, averaged over all 1005 runs.

but in most cases the escaper would drag some stars. In principle one can imagine one of these stars entering a giant phase and overflowing its Roche lobe, producing detectable accretion onto the SMBH long after its ejection from the galactic center.

3.4 Distant Evolution and Binary Re-formation

The slingshot ejections in triple SMBH encounters produce a population of “wandering” SMBHs in the halos of galaxies and intergalactic space (Volonteri et al. 2003a; Volonteri & Perna 2005). Fig. 14 shows the total time spent by the single (upper panel) and binary (lower panel) at various distances from the galactic center during the run time, averaged over all 1005 runs. The single is often found wandering at large distances, while the binary spends the vast majority of its time at the galactic center. Over all of our runs, the total fraction of the time spent with no SMBHs within 50 pc of the center since the formation of the halo hosting the triple system is only $\sim 1\%$. Hence we expect the ejections in triple-BH encounters at low redshift to produce very few nuclei empty of SMBHs. A cD galaxy cluster, having hosted several dry mergers, might contain up to a few naked SMBHs wandering through the cluster halo as a result of single ejections.

The escaper remains wandering through the halo in only $\sim 40\%$ of the runs. In the other cases dynamical friction brings it back to the center, where it becomes bound to the binary remnant and forms a new, hard binary. Fig. 15 shows the semi-major axis (upper panel) and eccentricity (lower panel) distributions of the “final state” binaries in our simulations. This plot includes binaries formed when a pair coalesces during a close encounter and is replaced by a single BH with its center-of-mass coordinates; cases where the original binary never coalesces, but rather settles to the center and stalls after the single escapes; and binaries that form from the third BH and coalesced remnant after ejec-

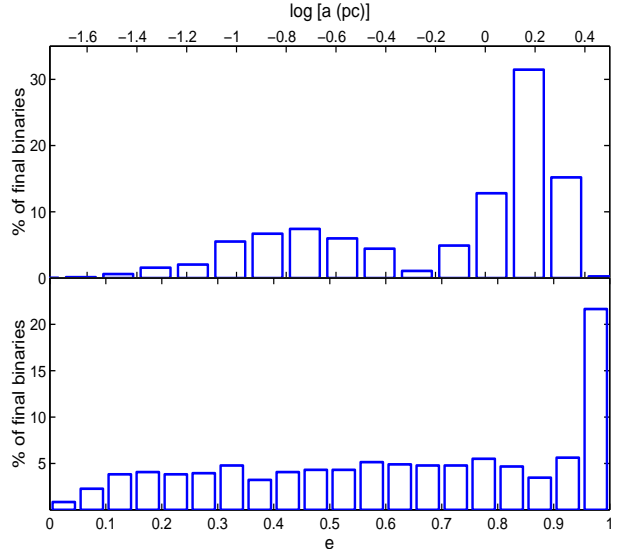


Figure 15. Distribution of parameters of “final state” binaries. The plot includes binaries that settled to the center after a single escape, and new binaries that formed from the single BH and inner binary remnant. Upper panel: Semi-major axis. Lower panel: Eccentricity.

tions. Whereas in the absence of triple encounters we would expect most SMBHs to sit around a_{hard} , the encounters introduce a second population of stalled binaries at smaller separations. The eccentricities of the final binaries span the whole range from 0 to 1. Note the peak at very high eccentricity, arising mostly from cases where the escaper rejoins the binary remnant from a radial orbit following a distant ejection, as in the run shown in the upper panel of Fig. 10.

In Fig. 16 we plot the total *time* spent by the binary at various semi-major axes and eccentricities, from the time of the merger that formed the original binary until the present day. The contribution from *before* the merger that formed the triple system is shown in blue. This phase just consists of a near-circular binary stalled at the hardening radius for a time $t_{f0} - t_{f1}$ in the notation of Fig. 4, the time between the merger that formed the binary and the merger that formed the triple system. The red histogram shows the (small) contribution from the binary evolution during the runs, and the green is the contribution from the “final state” binaries between the end of the run and $z = 0$. Note that the peak at $e \sim 1$ goes away in the time plot, since most of these very high-eccentricity systems coalesce quickly by gravitational radiation. This result has importance for LISA if three-body ejections are common enough, since the gravitational radiation signature of a highly eccentric binary is quite different from that of a circular binary. An eccentric binary radiates at all integer harmonics of the orbital frequency, so its spectral energy distribution peaks at higher frequencies, possibly enabling the detection of higher-mass SMBH binaries (e.g. Pierro et al. 2001; Enoki & Nagashima 2006).

However we caution the reader that the high-eccentricity coalescence rate appears to be sensitive to the dynamical friction and core updating prescriptions. We were able to change the re-formed binary coalescence rate significantly by varying our treatment of dynamical friction, and found the rate to decrease by a factor of 2-3

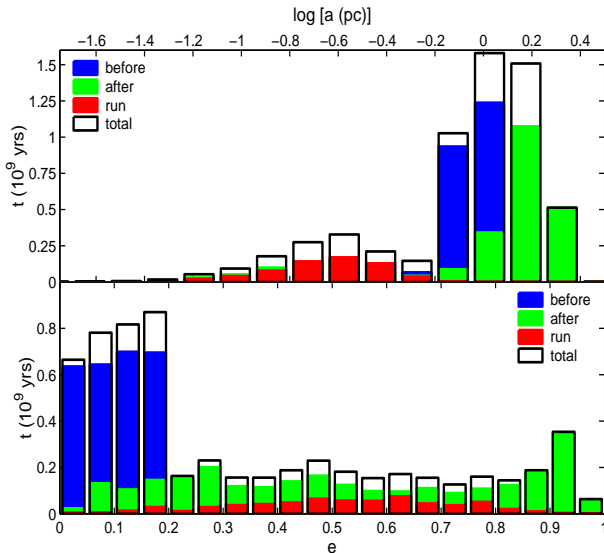


Figure 16. Total time spent by binaries at various semi-major axes and eccentricities, from the time of the merger that formed the binary until $z = 0$. Upper panel: Semi-major axis. Lower panel: Eccentricity. Blue filled: Contribution from before the merger that formed the triple system (binary sitting at a_{hard} over a time $t_{f0} - t_{f1}$ in the notation of Fig. 4). Red filled: Contribution from binary evolution during the run. Green filled: Contribution from final state binaries (as in Fig. 14) between the end of the run and $z = 0$. Black outline: Total. See text for further discussion.

when we turned off core updating. SMBH binary eccentricity evolution is a delicate question to which simulators have obtained widely discrepant answers (e.g. Aarseth 2003; Milosavljevic & Merritt 2001; Merritt & Milosavljević 2005). While the conclusion that a high-eccentricity population forms through distant ejections is robust, the question of whether these systems tend to coalesce or remain as an observable population of stalled high-eccentricity binaries may depend on the details.

3.5 Core creation

So far our discussion of stellar-BH interactions has focused on their effect on the BH orbits—tight binaries harden through stellar ejections and dynamical friction brings ejected BHs back to the galactic center. We now turn to the reverse effect of these interactions on the stars. Since the two-body relaxation time is long and there is little gas to make new stars in a dry merger, the mark left on the stellar distribution by a binary or multiple BH system persists long after the system reaches a steady state, e.g. by stalling or coalescence of the binary. This signature is observable even when the BHs cannot be detected more directly through their accretion processes.

A number of studies have addressed the mark left on a stellar core by the hardening of one or more BH binaries in independent succession (Milosavljevic & Merritt 2001; Ravindranath et al. 2002; Volonteri et al. 2003b; Merritt 2006). To estimate the damage, consider a succession of mergers $(M_0, M'_0) \rightarrow M_1, (M_1, M'_1) \rightarrow M_2, \dots, (M_{N-1}, M'_{N-1}) \rightarrow M_N$, between galaxies containing BHs of mass $(m_0, m'_0), \dots, (m_{N-1}, m'_{N-1})$, and having insuffi-

cient gas for significant stellar cusp regeneration. Suppose that following each merger the BHs spiral in to a_{hard} by dynamical friction on the stars, then cross the gap from a_{hard} to a_{gw} by some non-stellar mechanism, e.g. interaction with a modest amount of gas that ends up in the nucleus through tidal torques associated with the merger. The total energy deposited in the stellar core is roughly

$$E_{dep} \sim \sum_{i=0}^{N-1} \left(\frac{Gm_i m'_i}{a_{hard,i}} - \frac{Gm_i m'_i}{a_{inf,i}} \right), \quad (41)$$

where $a_{hard,i}$ is the hardening radius of the BH binary formed in each merger, and the radius of influence $a_{inf,i}$ is the radius containing about twice the mass of the larger binary member in stars (e.g. Merritt 2006). Note that the left-hand side of (41) is dominated by the first term in the parentheses, so the precise definition of $a_{inf,i}$ is not important. If the inner density profile of a galaxy flattens from $d\ln \rho / d\ln r = 3 - \eta$ to a shallower slope γ within some core radius r_b , then we can define a core “energy deficit” by

$$U_{def} = \pi \int_0^\infty [\rho(r)\Phi(r)r^2 - \rho_\eta(r)\Phi_\eta(r)r^2] dr, \quad (42)$$

the difference between the binding energy of the galaxy with the density break and that of the same galaxy, but with the density profile outside the core extrapolated inward to the center. In this equation $\rho = \rho_{stars} + \rho_{halo}$ and $\Phi = \Phi_{stars} + \Phi_{halo}$ denote the sums of the contributions to the density and gravitational potential from the stellar and dark matter halo components. The cross terms $\rho_{stars}\Phi_{halo}$ and $\rho_{halo}\Phi_{stars}$ contribute about 10-20% of the total binding energy, while the halo-halo terms are negligible. We denote the outer slope by $3 - \eta$ to match the Tremaine et al. (1994) parameterization used in our galactic models. We can estimate the size of the core created by the cumulative scouring action of the BH binaries formed in the succession of mergers by equating U_{def} of equation (42) to E_{dep} given by equation (41).

The $U_{def} = E_{dep}$ prescription was introduced in order to estimate the extent of cusp destruction *before the binary hardens*. If stalling were prevented by sufficient scattering of stars into the loss cone, an analogous energy argument would grossly overestimate the size of the core scoured out as the binary decayed from a_{hard} to the separation where gravitational radiation could take over. This is because a hard binary loses energy by ejecting stars at high velocities, often exceeding the escape velocity of the entire galaxy. Most of the energy released by the binary goes into excess kinetic energy of these hyper-velocity stars rather than heating of the local medium. Equations (41) and (42) capture the essence of the core scouring in the limit of weak encounters (dynamical friction), but for hard binaries we must view the cusp destruction as *mass ejection* rather than *energy injection*, once again following the work of Quinlan (1996). As discussed previously, a hard SMBH binary is defined by the fact that it hardens at a constant rate, $dE/dt = \text{const}$. In the limit of very high orbital velocity ($w \gg \sigma$) this implies that a constant mass in stars, comparable to the total BH mass, is ejected from the galactic center per e -folding of the binary semi-major axis,

$$\frac{1}{m_{bin}} \frac{dM_{ej}}{d\ln(1/a)} = \frac{1}{m_{bin}} \frac{dM_{ej}}{d\ln(E_{st})} \equiv J \approx 0.5, \quad (43)$$

where E_{st} is the energy transferred from the BH system to

the stars. We can estimate the core damage due to mass ejection by equating the total mass ejected by the binary to M_{def} as defined in equation (37).

Now suppose that instead of coalescing without further damaging the stellar core, the binary formed in the first merger in our sequence stalls at a_{hard} until a third BH sinks in following the second merger. On the one hand, some energy that would have been injected into the stars as the outer binary hardened may now instead be carried off as gravitational radiation or kinetic energy of a fast escaping BH, causing less damage to the stellar core than the decay of two separate binaries. On the other hand, the intruder may continue scattering stars into the loss cone well after the inner binary reaches a_{hard} , and ejected BHs heat the core by dynamical friction as their orbits pass repeatedly through the dense nucleus. The latter mechanism occurs only via the ejections following close three-body encounters, and may cause more efficient core growth per unit binding energy released from the binary than would ejection of high-velocity stars by a hard binary pair, as discussed above. Boylan-Kolchin et al. (2004) demonstrated the core-scouring effect of the dynamical friction on an ejected BH using full N-body simulations, with gravitational radiation recoil in mind. Radiation recoil is not important in the larger galaxies that we consider, but the repeated ejections in our simulations may cause greater cumulative heating. In this way multiple-BH interactions can create significantly larger cores than successive binary coalescences.

To quantify these considerations our code evolves the core radius r_b and slope γ along with the BH orbits to roughly account for the core heating and mass ejection caused by the triple systems. At the beginning of each run we initialize the core by injecting an energy

$$E_{init} = \frac{Gm_1m_2}{a_{hard,i}} + \frac{G(m_1+m_2)m_3}{a_{init,o}} - \frac{Gm_1m_2}{a_{inf,i}} + \frac{G(m_1+m_2)m_3}{a_{inf,o}} \quad (44)$$

into the parent η -model according to equation (42). In runs where the inner binary starts at $a > a_{hard}$ we replace $a_{hard,i}$ with $a_{init,i}$ in equation (44). In runs where it starts at $a < a_{hard}$ we also eject a mass $0.5m_{bin} \ln(a_{hard,i}/a_{init,i})$ according to equation (37) before the start of the run.

There is an ambiguity in the way we update the profile since energy may be injected (or mass may be ejected) either by increasing r_b to make the core larger, or by decreasing γ to make it shallower. We resolved this ambiguity by performing a rough fit to the γ vs. $y \equiv M_{def}/m_{bh}$ data in Merritt (2006), to obtain the relation

$$\gamma \approx -0.0281y^3 + 0.2451y^2 - 0.7094y + 1.000 \quad (45)$$

for $\eta = 2$, which gives sensible slopes for all $y \lesssim 5$. This relation at least has the desired property that $\gamma \rightarrow 3 - \eta$ as $M_{def} \rightarrow 0$, but the slope becomes quite shallow toward large M_{def} . The mass deficits are not sensitive to our prescription for γ .

During the unperturbed binary integration, we increment the energy injected at each timestep $t \rightarrow t + \Delta t$ by

$$\Delta E_{inj} = \sum_{i=1}^2 \int_t^{t+\Delta t} (\vec{F}_{df,i} \cdot \vec{v}_i) \theta(r_{core} - r_i) dt, \quad (46)$$

the work done on the single BH and binary center-of-mass by dynamical friction while the respective masses are located

within a distance $r_{core} \equiv 1.5r_b$ of the galactic center. When the binary is located within r_{core} and has not yet coalesced or settled to the center and stalled, we also increment the ejected mass by

$$\Delta M_{ej} = 0.5m_{bin} \ln \left(\frac{E_0 + \Delta E_{st}}{E_0} \right) \quad (47)$$

at each timestep, where E_0 is the binding energy of the binary at the beginning of the timestep and ΔE_{st} is the change in binding energy due to stellar hardening during that step. We cannot simply use the semi-major axis increment in equation (47) since the binary may also have hardened by gravitational radiation during the timestep.

During close encounters we label each pair as “instantaneously” hard or soft at the beginning of each Bulirsch-Stoer step by comparing its binding energy E_0 to $E_{hard} = Gm_1m_2/(2a_{hard})$. If the pair is bound with $|E_0| \leq E_{hard}$ then we update ΔE_{inj} according to equation (46). If $|E_0| > E_{hard}$ then we update ΔM_{ej} by equation (47), although during close encounters ΔE_{st} is computed using equation (28) (or not at all after the first encounter in prescriptions where we shut off dynamical friction at the onset of strong interactions). If the closest pair switches during a timestep or a pair is instantaneously hyperbolic ($E_0 > 0$) then we do not update ΔE_{inj} or ΔM_{ej} for that pair at that step (since the triple is hierarchical for most of the time even during close encounters, these steps do not matter).

Each time the total energy injected reaches 1% of E_{hard} or the total mass injected reached 1% of the total BH mass we update the core accordingly. At the end of each run we record the final M_{def} , r_b , and γ . Though both mass ejection and energy injection enter into our core growth algorithm, at the end both translate into a single effective M_{def} as given by equation (37), which we record for comparison with observed galaxies.

Fig. 17 shows the growth of the core with time in one of our runs with final $M_{def} = 1.88$. The upper panel shows the entire run history plotted as in Fig. 10, with the total physical time spent in each code stage normalized to one and the actual times (in yrs) marked on the figure. The lower panel displays the simultaneous evolution of the core mass deficit (in units of the total BH mass) and the density at the BH radius of influence. The core begins with $M_{def}/m_{bh} = 0.59$, and grows to $M_{def}/m_{bh} = 0.67$ during the first encounter. M_{def} increases to $0.87m_{bh}$ over the next 1.5×10^7 yrs as the single BH reaches a series of peaks at ~ 0.1 kpc separated by weak encounters with the binary. Then at $t = 1.8 \times 10^7$ yrs a strong encounter occurs (a $\Delta BE = 32\%$ increase in the binding energy from an initial $a_{in,0} = 0.70$ pc), resulting in ejection of the lightest BH to ~ 30 kpc, and growth of the core to $M_{def}/m_{bh} = 1.57$ by the time dynamical friction brings it back. The binary recoils to a distance of ~ 0.1 kpc, and the initial jump in M_{def} at this stage is due to the energy injected during the decay of its orbit and mass ejected as it hardens while wandering about the core. At $t = 5.2 \times 10^9$ yrs the three BH undergo another strong encounter ($\Delta BE = 7.3\%$ from $a_{in,0} = 0.019$ pc) an initial $a_{in,0} = 0.19$ pc), and M_{def}/m_{bh} increases to a final value of 1.88 as a result of this ejection. The binary finally coalesces 9.4×10^7 yrs after this last encounter. The third BH becomes bound to the binary remnant at $t = 7.1 \times 10^9$, and the new system coalesces with a final eccentricity of $e \approx 0.9984$ before

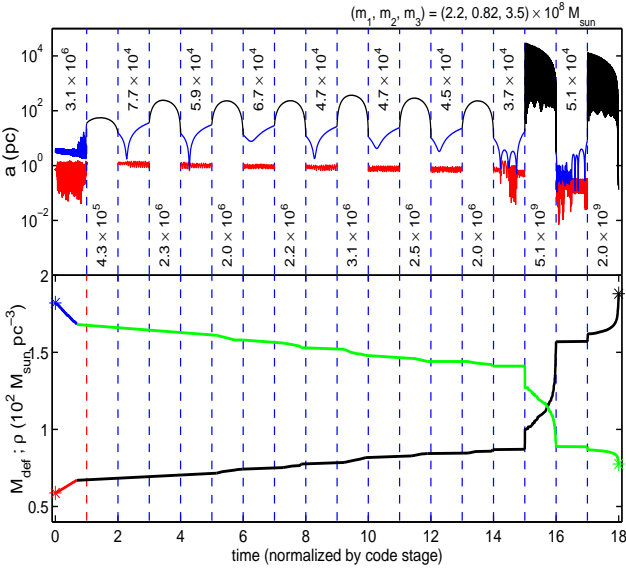


Figure 17. Core evolution over the course of a run with final $m_{def}/m_{bh} = 1.88$. Upper panel: Run history, plotted as in Fig. 10, with the time for each code stage normalized to one and actual times (in yrs) indicated on the plot. Lower panel: Simultaneous core evolution. The upper (green) curve shows the evolution of the density at the BH radius of influence, $r_{inf} = Gm_{bh}/\sigma^2$; the lower (black) curve shows the evolution of the core mass deficit, in units of the total BH mass. The contribution from the first encounter is plotted in different colors (blue and red). The asterisks highlight the initial and final values.

it reaches a_{hard} . In similar runs with slightly lower final eccentricity, the core gains an additional $\sim 0.5m_{bh}$ as the new binary hardens.

Fig. 18 shows the distribution of mass deficits and core radii predicted by our core scouring model for a series of two dry mergers. The blue (left) histogram is the distribution at the beginning of the runs, reflecting the heating of the core by dynamical friction on the BHs as they sink into the initial configuration with the inner binary at a_{hard} , equation (44). This distribution also approximately represents the core damage expected for a single merger in which stellar hardening ceases at a_{hard} . Note that a significant core ($M_{def}/m_{bh} \sim 0.5$) is scoured out even before the binary hardens and begins ejecting stars. The middle (black dashed) histogram shows the core predicted for a series of two dry mergers, in both of which stellar hardening stops at a_{hard} . The red (right) histogram is the distribution of cores at the end of our runs, reflecting the core scouring effect of the three-body interactions. We present the break radii in the lower panel to give the reader a feel for the relevant scales, but note that this distribution is specific to the typical BH mass ($m_{bh} \sim 6 \times 10^8 M_{\odot}$) and central density used in our runs, $r_b \sim (m_{bh}/\rho_{core})^{1/2}$. Observed galaxies will have a much wider range of break radii, though the mass deficits normalized to m_{bh} should be roughly independent of the scale and density profile.

In Fig. 19 we compare our calculations to 14 cored, luminous elliptical galaxies with BH masses ranging from $\sim 10^8 - 3 \times 10^9 M_{\odot}$, with measured mass deficits. The mass deficits are obtained in Graham (2004) and Ferrarese et al. (2006) by fitting the outer nuclear density profile to a Sérsic

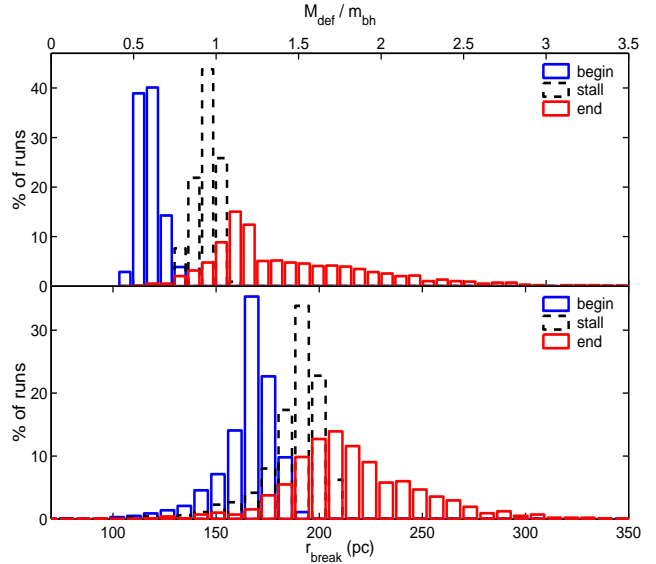


Figure 18. Mass deficits and core radii produced by SMBH scouring action in our model. Upper panel: Mass deficits in units of the total BH mass, $m_1 + m_2 + m_3$. Lower panel: Core radii in pc, for the Hernquist profile and BH mass scale of $\sim 6 \times 10^8 M_{\odot}$ adopted in our canonical runs. Blue (left): Beginning of simulation, based on core heating during inspiral to the initial configuration. Black dashed (middle): Net effect of two dry mergers in which core scouring stops at a_{hard} . Red (right): End of simulation, reflecting net energy injection and mass ejection caused by close triple encounters.

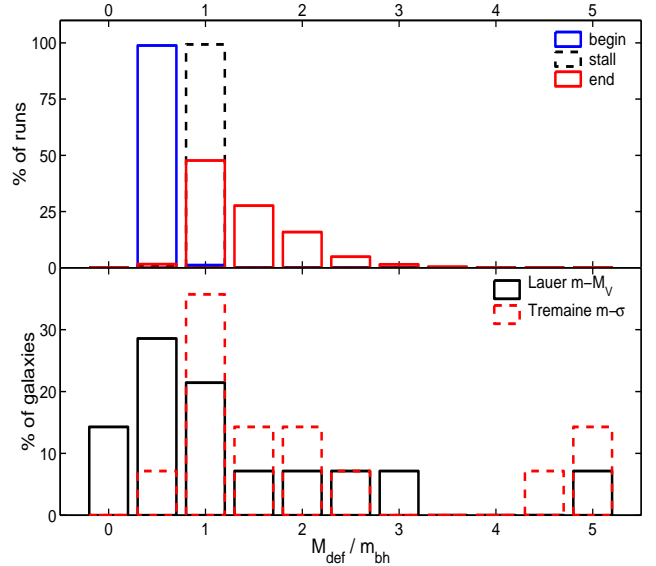


Figure 19. Comparison of calculated and observed mass deficits. Upper panel: Same as upper panel of Fig. 18, rebinned to accommodate small number of observed mass deficits. Lower panel: Observed mass deficits in units of the SMBH mass (Graham 2004; Ferrarese et al. 2006). In the red dashed histogram we determine the BH masses from the $m - \sigma$ relation of Tremaine et al. (2002), for all entries. In the black solid histogram we instead use the $m - M_V$ relation of Lauer et al. (2006) for those galaxies with $M_V < -22$, and the dynamically measured BH masses in the four cases where they are available.

Table 2. Mass deficits in galaxies with dynamically measured SMBH masses. References: Gebhardt et al. 2003 (G03), Bower et al. 1998 (B98), Macchetto et al. 1997 (M97), and Harms et al. 1994 (H94).

Galaxy	m_{bh}/M_{\odot}	M_V	M_{def}/m_{bh}	Reference
NGC 4291	3.1×10^8	-20.64	1.8	G03
NGC 4374	1.6×10^9	-22.28	1.4	B98
NGC 4486	3.0×10^9	-22.71	2.9	M97, H94
NGC 4649	2.0×10^9	-22.51	1.1	G03

law, and then subtracting a power-law fit to the inner core from the inward extrapolation of the Sérsic profile. The upper panel of Fig. 19 reproduces that of Fig. 18, but with the data rebinned to intervals of $\Delta M_{def}/m_{bh} = 0.5$ to accomodate the small number of observed data points. This binning is also natural since successive dry mergers where stellar hardening shuts off at a_{hard} result in a mass deficit of $\sim 0.5m_{bh}$ per merger. The red dashed histogram in the lower panel shows the observed M_{def}/m_{bh} with m_{bh} computed from the $M - \sigma$ relation of Tremaine et al. (2002). However Lauer et al. (2006) argue that luminosity may be a better predictor of BH mass than σ for the most luminous elliptical galaxies ($M_V \lesssim -22$), since their recent merger histories consisted mostly of passive (dry) mergers in which both the BH mass and luminosity are simply additive. The $M - \sigma$ relation is thought to arise from self-regulation of accretion onto the SMBH in gaseous mergers (Silk & Rees 1998; Wyithe & Loeb 2003b), which does not apply in this context. Lauer et al. (2006) also show that an extrapolation of the $m_{bh} - L$ relation to the highest luminosities is more consistent with the observed $r_{core} - m_{bh}$ relation and provides a better match between the $z = 0$ SMBH space density and the quasar population seen at $z \sim 2$ for reasonable quasar duty cycles. In the black histogram, we used the observed BH masses for the four cases with dynamical mass measurements (Gebhardt et al. 2003; Bower et al. 1998; Macchetto et al. 1997; Harms et al. 1994). For the rest of the galaxies we used the Lauer et al. (2006) $m_{bh} - M_V$ relation to estimate the BH masses in galaxies with $M_V < -22$, and the Tremaine et al. (2002) $M - \sigma$ relation for those with $M_V > -22$. Showing both plots gives an idea of how much the mass deficits vary with m_{bh} estimator².

In our canonical set CN $\sim 11\%$ of the runs resulted in cores with $M_{def}/m_{bh} > 2$. In some rare runs where the binary was ejected to a large distance and then brought back by dynamical friction, we obtained even higher mass deficits (up to $M_{def}/m_{bh} \sim 3 - 4$). The binary is more efficient at core scouring than the single BH since it is more massive. If each independent binary inspiral adds $\sim 0.5m_{bh}$ to the mass deficit, then the mean M_{def} enhancement of $\sim 0.5m_{bh}$ due to the triple encounters is equivalent to one extra merger in the system's history. An M_{def} one standard deviation above the mean is equivalent to two extra mergers. Note

² The Ferrarese & Merritt (2000) form of the $m_{bh} - \sigma$ relation also gives a distribution peaked at mass deficits of $\sim 0.5 - 1$, similar to the black histogram. However with so few data points, these differences must be taken with a grain of salt

that our conservative stellar hardening prescription tends to underestimate the core damage somewhat.

4 DISCUSSION AND CONCLUSIONS

Triple-SMBH systems in galactic nuclei produce a range of phenomena and signatures rather different from those expected if no more than two SMBHs occupy them at a time. We have developed an efficient numerical method for following the evolution of three body systems in the centers of galaxies, and used it to explore the outcomes of such encounters in massive elliptical galaxies at low redshift.

We find a high efficiency of SMBH coalescence due to the encounters, providing a “last resort” solution to the final parsec problem. There is, however, a caveat in extending this result immediately to all BH masses. If we define a_{esc} to be the binary semi-major axis where escape of one BH first becomes likely ($Gm_{bin}/\beta a_{esc} = v_{esc}^2$ where β is a factor of order 10 for a Hernquist profile), then since $v_{esc} \propto \sigma$ we have $a_{esc} \propto m_{bin}/\sigma^2 \propto m_{bin}^{1/2}$ if m_{bin} obeys the $m - \sigma$ relation $m_{bin} \propto \sigma^4$, so $a_{esc}/a_{gw} \propto m_{bin}^{-1/4}$. In other words, at smaller BH masses, the lightest BH is more likely to escape the galaxy before driving the binary to coalescence by gravitational radiation. By focusing on massive galaxies we have chosen the systems where the binary is *least* likely to coalesce by other means (e.g. gas or massive perturbers), and *most* likely to coalesce in the next merger with the help of three-BH interactions. We may address the efficiency of triple-induced coalescence in much smaller-mass systems in future studies.

We find that close triple encounters can produce a population of high-eccentricity binaries, whose gravitational radiation signal could potentially be observable by LISA. Such signals originate from Kozai oscillations in hierarchical triples at high initial inclinations and highly eccentric binaries formed following distant ejections. As the eccentricity increases, the radiation spectrum peaks at progressively higher harmonics of the fundamental frequency, approaching a nearly flat spectrum as $e \rightarrow 1$ (Pierro et al. 2001; Enoki & Nagashima 2006). A circular $10^{8-9} M_{\odot}$ BH binary remains below the band of frequencies ($\sim 10^{-4} - 10^{-1}$ Hz) detectable by LISA throughout its inspiral, but the occurrence of high-eccentricity coalescences could extend LISA’s sensitivity into this mass range, or lengthen the duration of its sensitivity to $\sim 10^{6-7} M_{\odot}$ events. A highly eccentric binary produces a “spiky” waveform that looks quite different from that of a circular system (see Fig. 7 in Pierro et al. 2001). Gravitational radiation “spikes” at very close approaches during chaotic three-body interactions could also produce radiation bursts detectable by LISA.

If triple encounters are indeed limited to massive systems at low redshift, then the importance of these considerations is limited by the expected event rate in this mass range, assuming efficient coalescence. This rate is highly uncertain, ranging from $\sim 1/\text{yr}$ (Sesana et al. 2005) to $\sim 1/1000\text{yr}$ (Rhook & Wyithe 2005) depending on the merger and BH population model adopted. If 3-BH systems occur in other contexts, e.g. IMBHs in galactic nuclei or star clusters, then the phenomena we have discussed may be observationally relevant even if the high-mass SMBH event rate is low. A detailed look at the gravitational waveforms expected from

three-body encounters and their expected detection rates is an interesting topic for a future study.

The slingshot ejections in triple encounters produce a population of “wandering” SMBHs in and outside the halos of galaxies. In systems that have undergone several major dry mergers (e.g. cD galaxy systems), one might expect a few such ejected SMBHs to be floating in the vicinity. As of yet, no probable way of observing these wandering BHs has been proposed³. In principle one can imagine a star bound to the ejected SMBH entering a giant phase and overflowing its Roche lobe, producing some accretion onto the SMBH and an observable flare. Single ejections could also in principle affect BH-bulge correlations such as the $m_{bh} - \sigma$ relation, but since it is the lightest BH that gets ejected this effect would fall well within the observed scatter in the correlations for just one or two ejection events.

Triple interactions in galactic nuclei can have a large effect on the expected properties of stable SMBH binaries in the local universe. While many models of binary formation predict mostly circular binaries around a_{hard} , three-body encounters produce binaries at all eccentricities. They also create a population of stalled binaries at separations significantly smaller than a_{hard} but still larger than a_{gw} , as does any partial gap-crossing mechanism.

Better measurements and statistics on the mass deficits in cored elliptical galaxies may provide clues on the history of the nuclear SMBH activity in these systems. Triple BH encounters produce a highly scattered distribution of core sizes, with mass deficits up to $\sim 2 \times$ higher than expected for successive binary coalescences. The apparent peak at mass deficits of $\sim 0.5 - 1$ times the nuclear BH mass in observed cores may very tentatively hint that multiple-BH encounters are not the norm in these systems. This signature of binary or multiple-BH activity is appealing because (a) its duty cycle is the lifetime of the galaxy; (b) it is present whether binary pairs stall or coalesce; and (c) it can be observed even in the complete absence of radiative activity, such as disk accretion or jet production. However the interpretation of galaxy cores is complicated by multiple mergers, the possibility of partial stellar cusp regeneration from traces of cold gas, and observational complications such as projection effects in nonspherical galaxies and optimizing the fitting/extrapolation algorithm to best represent the mass deficit. There is a need for theoretical studies on the cores produced by SMBH mergers in triaxial galaxies, since triaxiality seems to be the most likely candidate for a gap-crossing mechanism in dry mergers between gas-poor, giant ellipticals. Inferring the nuclear histories of galaxies from their observed core properties will likely be a topic of much interest in the future.

ACKNOWLEDGEMENTS

We would like to thank Suvendra Dutta for technical help at the parallel computing center of the Institute for Theory and Computation (ITC), and Sverre Aarseth and Seppo Mikkola for making their N-body algorithms and codes available. We

³ Gravitational lensing is difficult to search for without knowing in advance the location of the BHs.

are also grateful to Scott Hughes, Michael Eracleous, Marta Volonteri, and Fred Rasio for useful discussions. This research was supported in part by an FQXi grant and Harvard university funds.

REFERENCES

Aarseth, S.J. 2003, *Ap&SS* 285, 367
 Barkana, R. & Loeb, A. 2001, *PhR*, 349, 125
 Berczik, P., Merritt, D., Spurzem, R., & Bischof, H. 2006, *ApJ*, 642, 21
 Begelman, M.C., Blandford, R.D., & Rees, M.J. 1980, *Nature*, 287, 25
 Binney, J. & Tremaine, S. 1987, *Galactic Dynamics* (Princeton, New Jersey: Princeton University Press)
 Blaes, O., Lee, M.H., & Socrates, A. 2002, *ApJ*, 578, 775
 Blanchet, L., Qusailah, M. S. S., & Will, C. M. 2005, *ApJ*, 635, 508
 Bond, J.R., Cole, S., Efstathiou, G., & Kaiser, N. 1991, *ApJ*, 379, 440
 Bower, G.C., et al. 1998, *ApJL*, 492, 111
 Boylan-Kolchin, M., Ma, C., & Quataert, E. 2004, *ApJ*, 613, 37
 Bulirsch, R. & Stoer, J. 1966, *NuMat*, 8, 1
 Bullock, J.S., Kolatt, T.S., Sigad, Y., Somerville, R.S., Kravtsov, A.V., Klypin, A.A., Primack, J.R., & Dekel, A. 2001, *MNRAS*, 321, 559
 Byrd, G.G., Sundelius, B., & Valtonen, M. 1987, *A&A*, 171, 16
 Carroll, S.M., Press, W.H., & Turner, E.L. 1992, *ARA&A*, 30, 499
 Centrella, J. M. 2006, to appear in conf. proc. for the Sixth International LISA Symposium, AIP; preprint [astro-ph/0609172](http://arxiv.org/abs/astro-ph/0609172)
 Chandrasekhar, S. 1943, *ApJ*, 97, 255
 Chatterjee, P., Hernquist, L., & Loeb, A. 2003, *ApJ*, 592, 32
 Cohn, H. & Kulsrud, R.M. 1978, *ApJ*, 226, 1087
 Colpi, M., Mayer, L., & Governato, F. 1999, *ApJ*, 525, 720
 Cowie, L.L., Songaila, A., Hu, E.M., & Cohen, J.G. 1996, *AJ*, 112, 839
 Cox, T.J., Dutta, S.N., Di Matteo, T., Hernquist, L., Hopkins, P.F., Robertson, B., & Springel, V. 2006, *ApJ*, 650, 791
 Damour, T., & Deruelle, N. 1981, *PhLA*, 87, 81
 de Zeeuw, P.T. & Carollo, C.M. 1996, *MNRAS*, 281, 1333
 Eisenstein, D.J. & Hu, W. 1998, *ApJ*, 496, 605
 Enoki, N. & Nagashima, M. 2006, *PThPh*, submitted, [arXiv:astro-ph/0609377](http://arxiv.org/abs/astro-ph/0609377)
 Eracleous, M. & Halpern, J.P. 2003, *ApJ*, 599, 886
 Eracleous, M., Livio, M., Halpern, J.P., & Storch-Bergmann, T. 1995, *ApJ*, 438, 610
 Erickcek, A.L., Kamionkowski, M., & Benson, A.J. 2006, *MNRAS*, in press, [arXiv:astro-ph/0604281](http://arxiv.org/abs/astro-ph/0604281)
 Escala, A., Larson, R.B., Coppi, P.S., & Mardones, D. 2005, *ApJ*, 630, 152
 Escala, A., Larson, R.B., Coppi, P.S., & Mardones, D. 2004, *ApJ*, 607, 765

Favata, M., Hughes, S.A., & Holz, D.E. 2004, *ApJ*, 607, 5

Ferrarese, L. 2002, *ApJ*, 578, 90

Ferrarese, L., et al. 2006, *ApJS*, in press, arXiv:astroph/0602297

Ferrarese, L. & Merritt, D. 2000, *ApJ*, 539, L9

Frank, J., King, A., & Raine, D. 2002, *Accretion Power in Astrophysics*, 3rd Edition (Cambridge: Cambridge University Press)

Frank, J. & Rees, M.J. 1976, 176, 633

Gaskell, C.M. 1996, *ApJL*, 464, 107

Gebhardt, K., et al. 2000, *ApJ*, 539, L13

Gebhardt, K., et al. 2003, *ApJ*, 583, 92

Graham, A.W. 2004, *ApJ*, 613, 33

Gultekin, K., Miller, M.C., & Hamilton, D.P. 2006, *ApJ*, 640, 156

Haiman, Z. 2004, *ApJ*, 613, 36

Hao, C.N., Mao, S., Deng, Z.G., Xia, X.Y., & Wu, H. 2006, *MNRAS*, 370, 1339

Harms, R.J., et al. 1994, *ApJL*, 435, 35

Hayasaki, K., Mineshige, S., & Sudou, H. 2006, *PASJ*, submitted, arXiv:astroph/0609144

Hernquist, L. 1989, *Nature*, 340, 687

Hernquist, L. 1990, *ApJ*, 356, 359

Hills, J.G. & Fullerton, L.W. 1980, *AJ*, 85, 1281

Hoffman, L., & Loeb, A. 2006, *ApJL*, 638, L75

Holley-Bockelmann, K., Mihos, J.C., Sigurdson, S., Hernquist, L., & Norman, C. 2002, *ApJ*, 567, 817

Holman, M., Touma, J., & Tremaine, S. 1997, *Nature*, 386, 254

Hopman, C. & Alexander, T. 2006, *ApJ*, 645, 1152

Hut, P. & Bahcall, J.N. 1983, *ApJ*, 268, 319

Iwasawa, M., Funato, Y., & Makino, J. 2005, arXiv:astroph/0511391

Kitayama, T. & Suto, Y. 1996, *ApJ*, 469, 480

Komossa, S. 2003, arXiv:astroph/0306439

Komossa, S., Burwitz, V., Guenther, H., Predehl, P., Kaastra, J.S., & Ikebe, Y. 2003, *ApJ*, 582, 15

Kormendy, J. & Bender, R. 1996, *ApJL*, 464, 119

Kormendy, J. & Gebhardt, K. 2001, in 20th Texas Symposium on Relativistic Astrophysics, ed. J.C. Wheeler & H. Martel (Melville: AIP), 363

Kozai, Y. 1962, *AJ*, 67, 591

Kupi, G., Amaro-Seoane, P., & Spurzem, R. 2006, *MNRAS*, in press, arXiv:astroph/0602125

Kustaanheimo, P. & Stiefel 1965, *ApJ*, 97, 255

Lacey, C. & Cole, S. 1993, *MNRAS*, 262, 627

Lauer, T.R., et al. 2006, arXiv:astroph/0606739

Lauer, T.R., et al. 2006, arXiv:astroph/0606762

Lee, M.H. 1993, *ApJ*, 418, 147

Lightman, A.P., & Shapiro, S.L. 1977, *ApJ*, 211, 244

Macchetto, F., Marconi, A., Axon, D.J., Capetti, A., Sparks, W., & Crane, P. 1997, *ApJ*, 489, 579

Magorrian, J., et al. 1998, *AJ*, 115, 2285

Manrique, A. & Salvador-Sole, E. 1996, *ApJ*, 467, 504

Maoz, D., Filippenko, A.V., Ho, L.C., Rix, H.-W., Bahcall, J.N., Schneider, D.P., & Macchetto, F.D. 1995, *ApJ*, 440, 91

Maoz, D., Nagar, N.M., Falcke, H., & Wilson, A.S. 2005, *ApJ*, 625, 699

Marconi, A. & Hunt, L.K. 2003, *AJ*, 589, L21

Mardling, R. & Aarseth, S. 2001, *MNRAS*, 321, 398

Merritt, D. 2006, arXiv:astroph/0603439

Merritt, D., Milosavljevic, M., Favata, M., Hughes, S.A., & Holz, D.E. 2004, *ApJ*, 607, 9

Merritt, D., & Milosavljević, M. 2005, *Living Reviews in Relativity*, 8, 8

Merritt, D. & Ekers, R.D. 2002, *Science*, 297, 1310

Merritt, D. & Poon, M.Y. 2004, *ApJ*, 606, 788

Merritt, D. & Quinlan, G.D., *ApJ*, 498, 625

Mikkola, S. & Aarseth, S. 1990, *CeMDA*, 47, 375

Mikkola, S. & Aarseth, S. 1993, *CeMDA*, 57, 439

Milosavljevic, M. & Merritt, D. 2001, *ApJ*, 563, 34

Milosavljevic, M. & Merritt, D. 2003, *ApJ*, 596, 860

Naab, T., Khochfar, S., & Burkert, A. 2006, *ApJ*, 636, 81

Narayan, R., Theory of Thin Accretion Disks, course notes distributed in Astronomy 219, Spring 2003, Harvard University

Navarro, J.F., Frenk, C.S., & White, S.D.M. 1997, *ApJ*, 490, 493

Peng, C.Y., Impey, C.D., Ho, L.C., Barton, E.J., & Rix, H. 2006, *ApJ*, 640, 114

Perets, H.B., Hopman, C., & Alexander, T. 2006, *ApJ*, submitted, arXiv:astroph/0606443

Peters, P.C. 1964, *PhRv*, 136, 1224

Pierro, V., Pinto, I.M., Spallicci, A.D., Laserra, E., & Recano, F. 2001, *MNRAS*, 325, 358

Press, W.H. & Schechter, P. 1974, *ApJ*, 187, 425

Pursimo et al. 2000, *A&AS*, 146, 141

Quinlan, G.D. 1996, *NewA*, 1, 35

Quinlan, G.D., & Hernquist, L. 1997, *NewA*, 2, 533

Raig, A., Gonzalez-Casado, G., & Salvador-Sole, E. 2001, *MNRAS*, 327, 939

Ravindranath, S., Ho, C., & Filippenko, A.V. 2002, *ApJ*, 566, 801

Rhook, K.J., & Wyithe, J.S.B., *MNRAS*, 361, 1145

Rieger, F.M. 2006, arXiv:astroph/0611224

Rodriguez, C., Taylor, G.B., Zavala, R.T., Peck, A.B., Pollock, L.K., & Romani, R.W. 2006, *ApJ*, 646, 49

Roos, N. 1981, *A&A*, 104, 218

Roos, N., Kaastra, J.S., & Hummel, C.A. 1993, *ApJ*, 409, 130

Salpeter, E.E. 1964, *ApJ*, 140, 796

Salvador-Sole, E., Solanes, J.M., & Manrique, A. 1998, *ApJ*, 499, 542

Sanders, D.B., Soifer, B.T., Elias, J.H., Madore, B.F., Matthews, K., Neugebauer, G., & Scoville, N.Z. 1988, *ApJ*, 325, 74

Sérsic, J.L. 1968, Cordoba, Argentina: Observatorio Astronomico, 1968

Sesana, A., Haardt, F., Madau, P., & Volonteri, M. 2005, *ApJ*, 623, 23

Shakura, N.I., & Sunyaev, R.A. 1973, *A&A*, 24, 337

Shapiro, S.L. & Teukolsky, S.A. 1983, *Black Holes, White Dwarfs, and Neutron Stars: The Physics of Compact Objects* (Ithaca, New York: John Wiley & Sons)

Silk, J., & Rees, M.J. 1998, *A&A*, 331, L1

Sillanpaa, A., Haarala, S., Valtonen, M.J., Sundelius, B., & Byrd, G.G. 1988, *ApJ*, 325, 628

Sillanpaa et al. 1996, *A&A*, 305, 17

Spergel, D. et al. 2006, arXiv:astroph/0603449

Spitzer, L. 1987, *Dynamical Evolution of Globular Clusters* (Princeton, New Jersey: Princeton University Press)

Springel, V., Di Matteo, T., & Hernquist, L. 2005, *MNRAS*, 361, 776

Stiefel, E.L. & Scheifele, G. 1971, Linear and Regular Celestial Mechanics (New York: Springer-Verlag)

Stockton, A. & Farnham, T. 1991, *ApJ*, 371, 525

Taffoni, G., Mayer, L., Colpi, M., & Governato, F. 2003, *MNRAS*, 341, 434

Tremaine, S., Richstone, D.O., Byun, Y., Dressler, A., Faber, S.M., Grillmair, C., Kormendy, J., & Lauer, T.R. 1994, *AJ*, 107, 634

Tremaine, S., et al. 2002, *ApJ*, 574, 740

Valtaoja, E., Terasranta, H., Tornikoski, M., Sillanpaa, A., Aller, M.F., Aller, H.D., & Hughes, P.A. 2000, *ApJ*, 531, 744

Valtaoja, L. & Valtonen, M.J. 1989, *ApJ*, 343, 47

Valtonen, M.J., Mikkola, S., Heinamaki, P., & Valtonen, H. 1994, *ApJS*, 95, 69

Volonteri, M., Haardt, F., & Madau, P. 2003, *ApJ*, 582, 559

Volonteri, M., Madau, P., & Haardt, F. 2003, *ApJ*, 593, 661

Volonteri, M. & Perna, R. 2005, *MNRAS*, 358, 913

Wyithe, J.S.B. & Loeb, A. 2003, *ApJ*, 590, 691

Wyithe, J.S.B. & Loeb, A. 2003, *ApJ*, 595, 614

Wyithe, J.S.B. & Loeb, A. 2005, *ApJ*, 634, 910

Yu, Q. 2002, *MNRAS*, 331, 935